CHALMERS
UNIVERSITY OF TECHNOLOGY

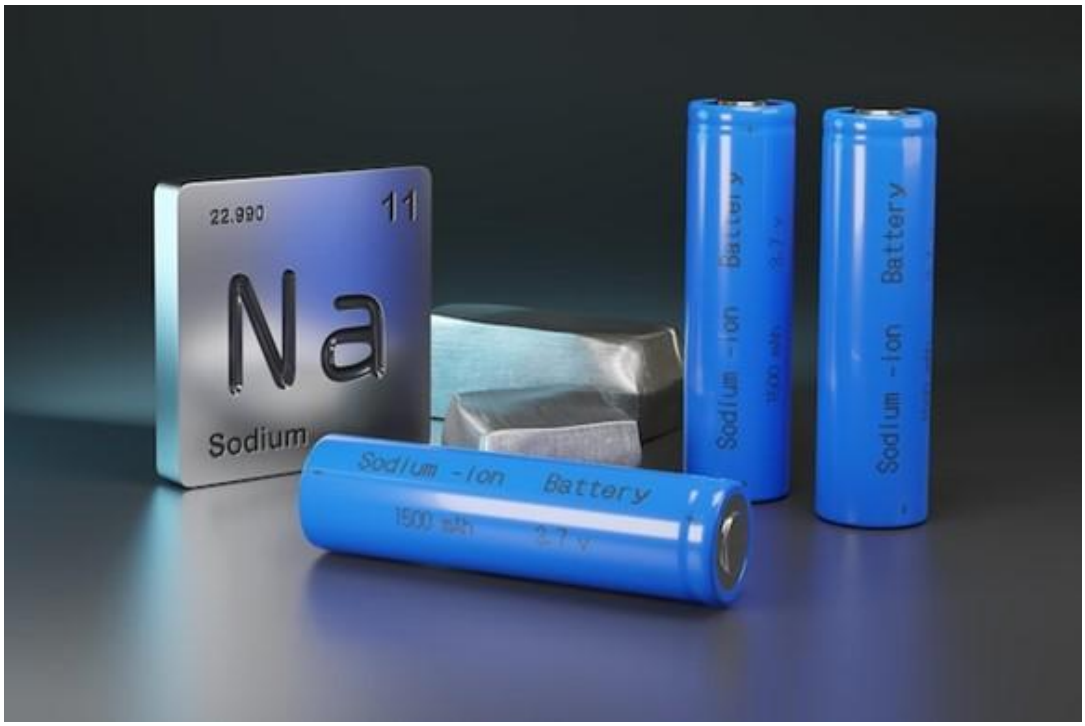

Optimized Synthesis of Multi Metal Prussian Blue Analogues Towards Stable Sodium-Ion Battery Cathode

Master's thesis in
Industrial and Materials Science

Prateek Mohan

DEPARTMENT OF INDUSTRIAL AND MATERIALS SCIENCE

CHALMERS UNIVERSITY OF TECHNOLOGY
Gothenburg, Sweden 2025
www.chalmers.se

MASTER'S THESIS IN INDUSTRIAL AND MATERIALS SCIENCE

Optimized Synthesis of Multi Metal Prussian Blue Analogues towards Stable Sodium-Ion Battery Cathode

CHALMERS
UNIVERSITY OF TECHNOLOGY

PRATEEK MOHAN

Department of Industrial and Materials Science
Division of Sustainable Energy Systems
CHALMERS UNIVERSITY OF TECHNOLOGY
Göteborg, Sweden 2026

Optimized Synthesis of Multi Metal Prussian Blue Analogues towards Stable Sodium-Ion Battery Cathode

PRATEEK MOHAN

Supervisor: Dr Nitish Kumar, Industrial and Materials Science
Examiner: Dr Jinhua Sun, Industrial and Materials Science

Department of Industrial and Materials Science
Division of Sustainable Energy Systems
Chalmers University of Technology
SE-412 96 Göteborg
Sweden
Telephone: + 46 (0)31-772 1000

Cover:
Illustration of Sodium-Ion battery cells representing the next-generation alternative to lithium-based systems.

Department of Industrial and Materials Science
Göteborg, Sweden 2026-01-22

Optimized Synthesis of Multi Metal Prussian Blue Analogues towards Stable Sodium-Ion Battery Cathode
Master’s thesis in the Master’s programme Industrial and Materials Science
PRATEEK MOHAN
Department of Industrial and Materials Science
Division of Sustainable Energy Systems
Chalmers University of Technology

Abstract

Sodium-ion batteries are increasingly considered a viable alternative to lithium-ion systems for large-scale (stationary) energy storage due to the abundance and low cost of sodium. Among potential cathode materials, Prussian Blue Analogues (PBAs) offer fast sodium-ion diffusion and high operating voltages but often suffer from structural instability and capacity fading during long-term cycling. In this study, multi-metal Prussian Blue Analogues are developed to overcome these limitations by stabilising the framework and enhancing electrochemical performance through synergistic interactions between multiple transition metals. The materials were synthesised using controlled co-precipitation and hydrothermal methods, enabling precise control over composition, morphology, and defect concentration. Structural and electrochemical characterisation using X-ray diffraction, scanning electron microscopy, cyclic voltammetry, galvanostatic charge–discharge testing, and electrochemical impedance spectroscopy demonstrates improved crystallinity, reduced polarisation, enhanced rate capability, and superior cycling stability compared with single-metal PBAs. The improved performance is attributed to enhanced redox activity and improved structural integrity during repeated sodium insertion and extraction. These results highlight multi-metal Prussian Blue Analogues as promising cathode materials for scalable and durable sodium-ion batteries intended for stationary and grid-level energy storage applications.

Keywords:

Sodium-ion batteries, Prussian Blue Analogues, Energy storage materials, Self-decomposition synthesis, Hydrothermal synthesis, Structure–property relationship

Preface

This thesis is a product of the Master's programme in Sustainable Energy Systems at Chalmers University of Technology and was completed during the academic year 2024–2025. The research presented in this work focuses on the optimised synthesis of multi-metal Prussian Blue Analogues towards stable cathode materials for sodium-ion battery applications, addressing key challenges related to material performance, sustainability, and scalability.

The project has been both challenging and intellectually rewarding, combining elements of materials science, electrochemistry, and energy storage engineering. Throughout this work, I was able to deepen my understanding of advanced battery materials while developing strong experimental, analytical, and problem-solving skills. In particular, the study offered valuable insight into how synthesis strategies influence structural properties and electrochemical behaviour, which are critical for the development of next-generation energy storage technologies.This thesis has also contributed to a broader appreciation of the role that alternative battery chemistries, such as sodium-ion systems, can play in supporting sustainable energy solutions. The knowledge gained through this work has strengthened my interest in battery research and reinforced the importance of materials innovation in addressing global energy challenges.

Acknowledgements

I would like to express my sincere gratitude to my supervisor, **Dr Nitish Kumar**, Postdoctoral Researcher**,** for their continuous guidance, encouragement, and constructive feedback throughout the course of this thesis. Their technical expertise, patience, and critical insights were invaluable in shaping the direction and quality of this research.

I would also like to thank **Dr Jinhua Sun,** from Industrial and Material Sciences, for their helpful discussions, thoughtful comments, and support, which significantly contributed to improving the scientific depth and clarity of this work.

My appreciation extends to my fellow students and colleagues for their collaboration, exchange of ideas, and positive working environment. I am especially grateful for the technical support provided in the laboratory, which ensured that the experimental work was carried out smoothly and efficiently.

Finally, I would like to express my heartfelt thanks to my family and friends for their unwavering support, patience, and motivation throughout my studies. Their constant encouragement and belief in me played a crucial role in helping me complete this thesis successfully.

Göteborg January 2026-01-22

PRATEEK MOHAN

Contents

List of figures

List of tables

1 Introduction

Energy is the backbone of essential activities such as transportation, healthcare, communication, and industrial production. As the world moves away from traditional, non-renewable energy sources and toward cleaner, renewable ones, the need for lightweight, efficient, and reliable energy-storage technology has grown a lot. Batteries are the most important option because they supply portable, flexible, and on-demand electricity. This makes it possible to electrify a wide range of products, from smartphones and laptops to electric cars and renewable energy grids. Batteries store energy as chemicals and turn it into electrical energy through reversible redox reactions between two electrodes—the anode and the cathode. An electrolyte separates the two electrodes and lets ions move while stopping electrons from moving, which lets the battery go through charge–discharge cycles over and over. Also, battery systems are very important for renewable energy sources like solar and wind since they help with power outages, make the grid more stable, and lower carbon emissions. As transportation becomes more electric in order to reduce carbon emissions from the grid, the need for batteries that have higher energy density, charge faster, are safer, and have less of an impact on the environment has grown. However, worries over the availability of lithium and its long-term viability have led researchers to look into next-generation sodium-ion batteries, which are becoming intriguing and more sustainable options to traditional lithium-ion technology. (1)

1.1 Evolution of Battery Technologies

The increased demand for efficient, dependable, and portable energy storage solutions has accelerated the progress of battery technology. Early batteries, such as the voltaic pile invented in the late 18th century, were the first to convert chemical energy into electrical energy, laying the groundwork for electrochemical power sources. This was followed by the invention of primary batteries, such as zinc-carbon and alkaline cells, which provided greater stability and usability but were limited by their single-use nature. The emergence of rechargeable secondary batteries, such as lead-acid and nickel-based systems, marked a significant step forward by allowing for many charge-discharge cycles and supporting applications in automobile and backup power systems. The development of lithium-ion batteries in the late twentieth century was a watershed moment due to their high energy density, long cycle life, and lightweight design, making them the primary technology for portable devices and electric vehicles. However, growing worries about resource scarcity, affordability, safety, and environmental sustainability have resulted in extensive research into alternative battery chemistry. As a result, next-generation systems such as sodium-ion, solid-state, and multivalent batteries are being actively researched to solve the limitations of current technologies and satisfy the energy-storage needs of a rapidly electrified and decarbonising global energy system. (2)

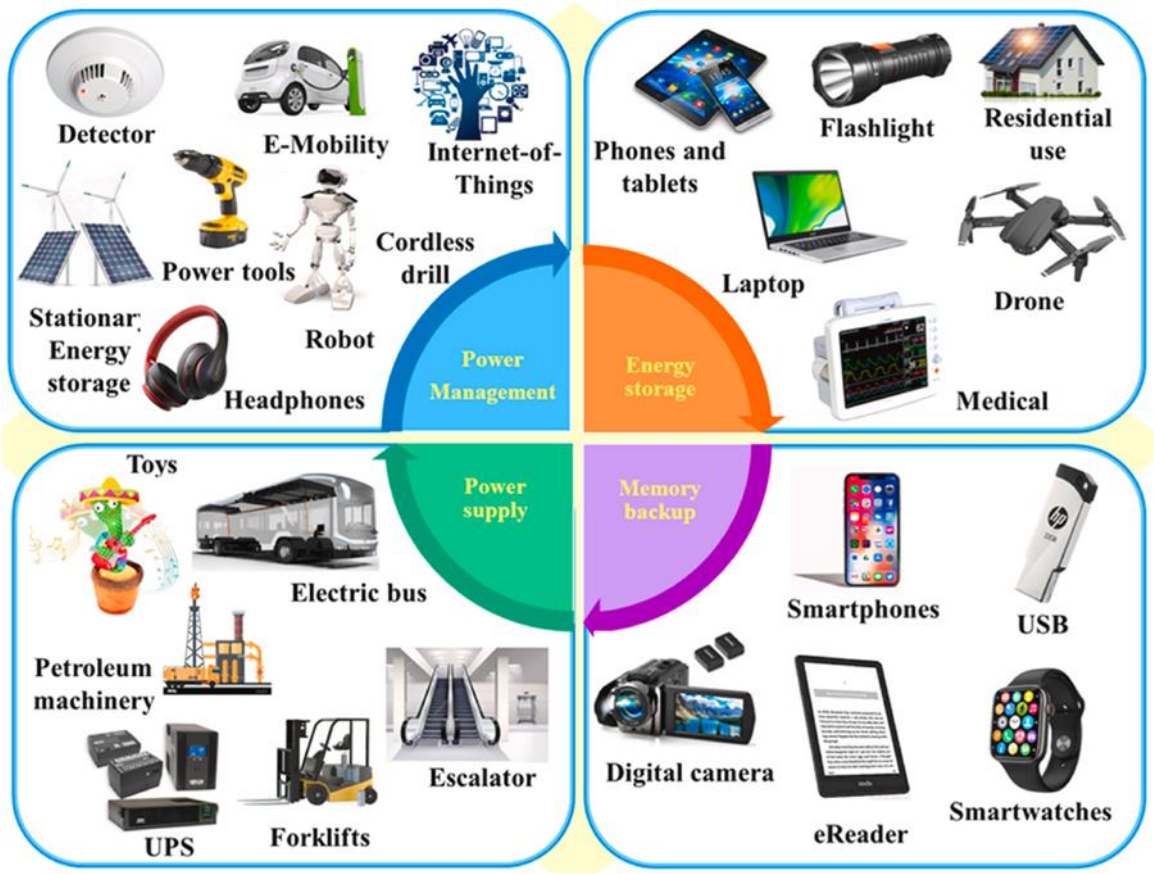

Figure 1- Application domains of rechargeable battery systems, highlighting power management, energy storage, power supply, and memory backup functions (Olabi et al., Energy 2023, 266, 126408.)

1.2 Global Energy Transition and the Role of Energy Storage

The global energy transition aims to achieve net-zero greenhouse gas emissions by mid-century. Much of the upcoming electricity will be generated using renewable energy. Nonetheless, sources like solar and wind are intermittent and uneven, resulting in a lack of continuity in generation and demand. Thus, energy-storage methods are essential to ensure control consistency, frequency regulation, and peak-load counterbalance. Batteries are a fantastic treatment option because of their quick response time and creative versatility in producing things at various scales, ranging from residential storage rooms to multi-megawatt grid installations. They have faster response times and turnaround efficiency than pumped hydro or compacted air storage. As a result, according to global forecasts, stationary storage capacity will exceed 2 TWh by 2030. Overall, this will be fueled by lithium and sodium ion batteries.

1.3 Working Principle of Rechargeable Batteries

Rechargeable batteries use reversible electrochemical reactions to store and release electrical energy on a regular schedule. During discharge, chemical energy held in the electrodes' active materials is transferred to electrical energy via oxidation and reduction reactions at the anode and cathode, respectively. Electrons produced at the anode flow via the external circuit to the cathode, generating usable electrical power, while charge neutrality is maintained by the simultaneous migration of ions through the electrolyte. During charging, an external electrical potential reverses these processes, causing ions to return to their original electrode and restoring the system's electrochemical energy. The electrolyte is important because it facilitates ionic transport while inhibiting direct electronic conduction between the electrodes, which prevents internal short circuits. A separator is often used to keep the electrodes physically apart while enabling ions to flow. The electrochemical stability of the electrode materials, ion transport kinetics, electrode-electrolyte interfacial behavior, and structural reversibility of the active materials during repeated charge-discharge cycles all influence rechargeable battery performance, including energy density, power capability, cycle life, and safety. (3).

1.4 Limitations of Current Lithium-Ion Technology

Lithium-ion batteries face several challenges limiting large-scale sustainability; first, lithium and cobalt reserves are non-ubiquitous – they are concentrated in South America, Australia, and the DRC, creating supply-chain vulnerabilities and price volatility. Moreover, cobalt mining has also caused numerous ethical and environmental concerns, whereas lithium extraction requires large amounts of water. Technically, LIBs are vulnerable to thermal runaway, electrolyte flammability, and capacity fading due to dendrite formation and dissolution of transition metals. Finally, recycling and end-of-life management of LIBs are underdeveloped, with less than 5% of global LIBs recycled efficiently. Combined, these issues necessitate the development of resource-abundant, safer, and more sustainable alternatives. (4)

1.5 Motivation for Sodium-Ion Batteries

Sodium-ion batteries provide a viable substitution for the limitations arising with the LIBs. The sodium, ranked as the sixth most concentrated element in Earth’s crust, can be abundantly sourced from seawater or rock salt at an economically sustainable price. This distinction supports long-term resource stability. Na^+ acquires similar electrochemical characteristics to those of Li^+; consequently, the two exhibit the same cell architecture and consummate compatibility. (5)

Sodium-ion batteries (SIBs exhibit marginally lower operating voltages compared to lithium-ion batteries, this difference arises from the less negative standard redox potential of sodium ($Na^+/Na = -2.71$ V vs. SHE) relative to lithium ($Li^+/Li = -3.04$ V vs. SHE), resulting in typical SIB cell voltages of approximately 2.5–3.5 V compared to 3.6–4.2 V for lithium-ion systems. Despite this inherent voltage limitation, SIBs are favoured due to the widespread availability of sodium, lower raw-material and extraction costs, improved thermal stability, reduced safety risks, and more reliable operation at elevated temperatures. Recent milestones in industrialisation, including prototype developments by Faradion Ltd., HiNa Battery, and CATL, demonstrate promising levels of technological maturity. Consequently, SIBs are increasingly

recognised as an economically viable solution for stationary energy storage, rural electrification, grid balancing applications, and short-range urban mobility, where cost efficiency, safety, and sustainability are prioritised over gravimetric energy density. (6)

1.6 Scope And Objectives of the Thesis

This thesis examines the theoretical and material foundations of sodium-ion batteries, with a particular focus on **Prussian Blue Analogues (PBA) cathodes** and their role in sustainable energy-storage systems. Chapter 2 presents the theoretical background, comparing sodium- and lithium-ion chemistries and exploring the structural, electrochemical, and practical characteristics of PBAs. Chapter 3 describes the methodology used to analyse the selected literature and empirical data, while Chapter 4 presents and discusses the key results. Chapter 5 concludes by summarising the main findings and highlighting opportunities for future research.

The overarching objectives are:

1. **To synthesise and systematically optimise multi-metal PBAs** incorporating multiple transition metals, to achieve structurally stable and electrochemically active cathode materials suitable for sodium-ion battery applications.

2. **To investigate and compare different synthesis routes for PBAs**, including co-precipitation, self-decomposition, and hydrothermal methods, to evaluate their efficiency, scalability, and sustainability with respect to material quality and processing conditions.

3. **To optimise slurry formulation and electrode coating parameters**, ensuring uniform dispersion of active material, appropriate binder distribution, and mechanically robust electrode films that enable reliable electrochemical testing.

4. **To evaluate the suitability of multi-metal PBAs as cathode materials** by employing a range of electrochemical characterisation techniques, such as galvanostatic charge–discharge cycling, cyclic voltammetry, and rate capability analysis.

5. **To compare the electrochemical performance of PBAs synthesised via different methods**, focusing on specific capacity, voltage profile, cycling stability, and rate performance, and to identify the synthesis approach that offers the most balanced overall battery performance.

2 THEORY

2.1 Fundamental Properties of Sodium and Comparison with Lithium

Although sodium and lithium both belong to the alkali metal group, their physical and electrochemical properties differ significantly. Sodium ions possess a larger ionic radius (1.02 Å) compared to lithium ions (0.76 Å), which prevents dense packing within conventional electrode structures and necessitates the use of more open host frameworks in sodium-ion batteries (SIBs). Despite this limitation, sodium offers several compelling advantages, including its high natural abundance, low extraction cost, and ease of recovery from widely available sources such as seawater and rock salt, along with lower reactivity toward moisture. In terms of electrochemical performance, SIBs typically operate at voltages of 2.5–3.5 V, compared to 3.6–4.2 V for lithium-ion batteries (LIBs), and deliver energy densities in the range of 120–180 Wh kg^{-1}, which are slightly lower than those of LIBs. However, SIBs exhibit improved thermal stability and enhanced safety characteristics, despite potential challenges related to electrolyte decomposition. Owing to these attributes, SIBs are particularly well suited for stationary energy storage and large-scale applications where low cost, safety, and material sustainability are prioritised over gravimetric energy density. (7)

A Sodium-ion battery is based on the same working principle as a lithium-ion battery; however, it uses Na^+ as the moving charge carriers, not Li^+. During charging and discharging, these ions shuttle back and forth between two electrodes through an electrolyte, and electrons travel through the external circuit to power a device. A typical sodium-ion cell component includes. In a sodium-ion battery (SIB), the anode is the electrode that oxidises during discharge. In the charged state, it serves as a sodium storage host, releasing sodium ions into the electrolyte upon discharge. Because sodium's high ionic radius hinders effective intercalation into graphite, hard carbon is frequently employed as an anode material. Its disordered structure, composed of turbostratic carbon layers and nanopores, allows for salt storage via adsorption and minimal intercalation. Alloy-type anodes, such as tin, antimony, and phosphorus, are also being studied due to their high theoretical capacities, albeit their practical application is limited by significant volume expansion during cycling.

The cathode serves as the positive electrode and is reduced during discharge. It is often made up of sodium-containing compounds, including layered transition metal oxides, polyanionic materials, and PBA's (PBAs). PBAs are particularly appealing due to their open framework structure, which allows for rapid sodium-ion diffusion while maintaining structural integrity. During discharge, sodium ions travel from the anode to the cathode via the electrolyte, while electrons flow through the external circuit. The electrolyte facilitates sodium-ion movement across electrodes while electrically isolating them. It can be liquid, gel, or solid, and it must have strong ionic conductivity, electrochemical stability across the operating voltage range, and chemical compatibility with both electrodes to guarantee efficient and stable battery operation. The separator is a thin, porous membrane that physically separates the anode and cathode, preventing short circuits while allowing sodium ions to travel freely. The separator helps to sustain ionic transport while also contributing to the battery's overall safety and mechanical

stability. When discharging occurs, sodium ions depart the anode and migrate through the electrolyte to the cathode electrode, where they are inserted into the crystal structure of the host material. Electrons liberated from the anode migrate through the outermost loop, creating electrical energy. When the battery is charged, an external power supply returns electrons to the anode and oppositely propels sodium ions. Because the ions forcibly "rock" back and forth between the electrodes, SIBs are generally referred to as rocking-chair batteries. (8)

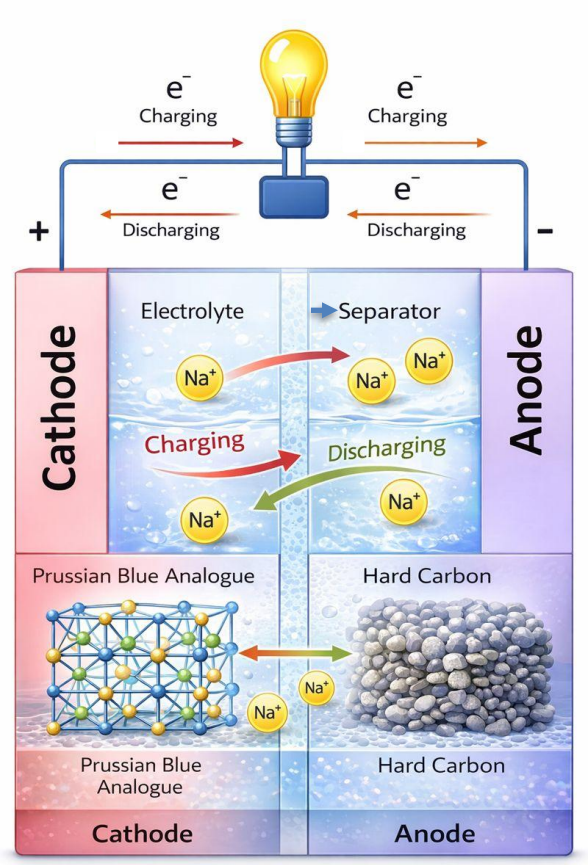

Figure 2 : Working schematic diagram of Sodium-ion Batteries*

2.1.1 Key Performance Parameters

A few standard measurements help evaluate battery performance:

- **Specific capacity (mAh g^{-1}):** the charge stored per gram of active material.
- **Energy density (Wh kg^{-1}):** the total energy delivered per unit mass, found by multiplying capacity and average voltage.
- **Power density (W kg^{-1}):** the rate at which energy can be released.
- **Coulombic efficiency (%):** the ratio of discharge to charge capacity, indicating reversibility (values close to 100 % are ideal).
- **Cycle life:** the number of charge–discharge cycles before the battery's capacity drops to 80 % of its original value.

These properties depend on the type of electrode materials used, particle size, ion-diffusion speed, and electrolyte stability.

2.2 Different Cathode Materials in Sodium-Ion Batteries

It is the cathode that largely determines how much energy a sodium-ion battery can deliver. At present, three main families prevail in this area of research: layered transition-metal oxides, polyanionic compounds, and PBA's [26, 29]. While all three store sodium via intercalation, they differ in structure and lifecycle.

Layered Transition-Metal Oxides $NaMO_2$

These compounds, with formula $NaMO_2$, where M= Fe, Mn, Ni, Co, etc., have different structural types, P2, O3, and P3, depending on the stacking of oxygen layers and sodium. P2-type O3-type Using prismatic sodium sites, P2-type $Na_{0.67}MnO_2$ shows good rate performances at room temperature, but its cathodes tend to become unstable at high states of charge. Octahedral O3 type, $NaFeO_2$, $NaMO_2$ has a higher capacity than the P2 form, but it reacts with the ambient air and moisture.Layered oxides can reach about 160-200 mAh g-1 at 3.0-3.8 V but suffer from the problem of irreversible phase transitions and oxygen release; while various doping and surface modifications alleviate this problem, they make synthesis more costly and complicated.

Polyanionic Compounds

Polyanionic cathodes. They are a subclass of $Na_3V_2(PO_4)_3$ and $NaFePO_4$. The frameworks are composed of durable covalent anion clusters (PO_4^{3-}, SO_4^{2-}, etc). The inductive effect of the cluster stabilises high-voltage redox couples, and the almost invariant voltage plateau is formed, which guarantees high safety. Voltage is 3.2–3.8 V, and capacity is 100–120 mAh g^{-1}. A low value of electronic conductivity is their disadvantage, which can be compensated for using carbon coatings and by reducing the size of active particles.

Prussian Blue Analogues

PBAs merge low cost and sustainability with good electrochemical performance (120–150 mAh g^{-1} at 3.2–3.6 V). Their simple water-based synthesis makes them particularly attractive for mass production and stationary energy storage.

Cathode Type	Example	Voltage (V)	Capacity (mAh g^{-1})	Strengths	Limitations
Layered oxides	$Na_{0.67}MnO_2$, $NaFeO_2$	3.0–3.8	160–200	High energy	Air sensitivity, phase changes
Polyanionic compounds	$Na_3V_2(PO_4)_3$, $NaFePO_4$	3.2–3.8	100–120	Stable, safe	Low conductivity
PBA	$Na_2Fe[Fe(CN)_6]$, $Na_xFe–Mn[Fe(CN)_6]$	3.2–3.6	120–150	Fast kinetics, low cost	Vacancies, moderate conductivity

Table 1- Comparison of key sodium-ion battery cathode materials showing their voltage ranges, capacities, strengths, and limitations.

2.3 Prussian Blue Analogues (PBAs): Structure and Electrochemical Mechanism

2.3.1 Prussian Blue Analogues

PBA's (PBAs) are open-framework coordination compounds with the generic formula $A_xM[M'\ (CN)_6]_\gamma \cdot nH_2O$, where A represents an alkali metal ion and M/M' are transition metals coupled by cyanide ligands. PBAs have a hard cubic crystal structure and extensive, interconnected diffusion channels, which allow for quick alkali-ion transport while maintaining structural integrity throughout repeated electrochemical cycling. These materials have received a lot of attention as cathodes for sodium-ion batteries because of their capacity to accommodate massive sodium ions, low diffusion barriers, and customizable electrochemical properties via compositional engineering. Furthermore, PBAs may be synthesized utilizing scalable, low-temperature solution-based processes, making them cost-effective for large-scale energy storage applications. The combination of structural openness, compositional flexibility, and favourable electrochemical behaviour makes PBAs intriguing candidates for next-generation sodium-ion battery cathodes.

2.3.2 Crystal Structure

PBA's (PBAs) form a family of transition-metal coordination compounds with an open cubic framework. Their general chemical formula is:

$$A_xM_1[M_2(CN)_6]_{1-y} \cdot nH_2O$$

where A is an alkali ion such as Na^+, M_1 and M_2 are transition metals like Fe, Mn, Ni, Co, or Cu, and y represents the fraction of $[Fe(CN)_6]$ vacancies.Each metal atom sits inside an octahedral cage of carbon or nitrogen atoms linked by cyanide bridges, creating a strong three-dimensional lattice. The open spaces between these octahedra act as channels for sodium-ion transport. The structure remains remarkably stable during cycling, showing volume changes of less than 3 %, which is crucial for long life.

2.3.3 Redox Process and Charge Storage

When a PBA is used as a cathode, sodium ions enter and leave the crystal lattice through a reversible redox process involving the Fe^{2+}/Fe^{3+} and M^{2+}/M^{3+} couples:

$$Na_{x-y}M_1[M_2(CN)_6] + yNa^+ + ye^- \rightarrow Na_xM_1[M_2(CN)_6]$$

Because the framework remains almost unchanged, the process is highly reversible. Depending on whether one or two electrons are involved, the theoretical capacity ranges from 85 to 170 mAh g^{-1}, with operating voltages around 3.2–3.6 V vs Na^+/Na.

2.3.4 Structure–Transport Properties, Defects, and Performance Implications of PBA's

PBA's (PBAs) have excellent electrical and ion-transport properties, making them ideal as cathode materials for sodium-ion batteries. The cyanide ligands in the PBA framework form extensive π-bonding networks, enabling partial electron

delocalisation and modest intrinsic electrical conductivity even before the application of conductive carbon coatings. PBAs have a cubic crystal structure with broad, linked channels of roughly 3.2 Å in diameter. This enables rapid sodium-ion diffusion with a low activation energy of approximately 0.3 eV, which is significantly lower than that of many oxide-based cathode materials. These qualities work together to give PBAs their excellent rate capacity and cycling stability. PBAs, on the other hand, are fundamentally faulty materials that often contain structural voids and water molecules. Missing $[Fe(CN)_6]$ units lead to fewer electrochemically active redox sites, while water can fill lattice holes or couple with metal centres. Although a small amount of water can improve crystallographic integrity, excess water weakens metal-cyanide bonding and increases self-degradation. As a result, careful control of synthesis parameters such as precursor concentration, solution pH, and drying temperature is required to achieve an ideal balance of conductivity and structural durability. Overall, PBAs are appealing due to their low cost, environmental friendliness, and ease of synthesis from plentiful basic materials. While challenges related to moisture sensitivity, intrinsic defects, and capacity loss remain, advances in multimetal substitution, surface modification, and coating strategies have significantly mitigated these limitations, reinforcing PBAs as one of the most promising cathode materials for future sodium-ion battery technologies.

2.4 Challenges and Opportunities with PBAs

Though PBAs possess a host of desirable properties, various technical obstacles stand in their way of being realised as fully commercially mature technologies (9). Structural defects via vacancies in $[Fe(CN)_6]$ groups reduce active redox sites, lowering capacity and stability. Managing reaction stoichiometry and crystal-growth are essential. Water exists as crystal-bound or adsorbed moisture; too much increases resistivity and promotes degradation, while too little causes lattice collapse. Proper hydration is critical. Metal leaching or, when transition metals such as Mn or Co dissolve into the electrolyte, fading capacity and composition alteration occur. Particle morphology with uneven sizes yields long ion-diffusion pathways; while uniform nanosized particles yield high kinetics, they may necessitate protective coatings against side reactions.Electronic conductivity, as they have intrinsically poor conductivity; applying carbon coatings or using conductive dopants, such as Ni or Co, helps. Thus, while their limited advancement suggests PBAs have a long way to go, they are perhaps the most promising cathode material as well. By combining defect control, surface modification, and ideal synthesis, PBAs can be further optimised for practical use in sodium-ion technology.

2.5 Multi-Metal PBA's: Design Principles and Electrochemical Benefits

In recent years, a greater amount of attention has been paid by researchers to the multi-metal Prussian Blue Analogues (PBA), referring to materials combining two or more transition metals sharing a similar crystal framework. The rationale behind this development is to employ the specific characteristics of each metal species to improve the overall electrochemical performance. The mixing of metals such as Fe, Mn, and Ni

and Co in the same lattice makes possible the generation of a set of synergistic redox couples operating over a broader potential range. For example, the Fe2+/Fe3+ and Mn2+/Mn3+ pairs can both be involved in preserving the charge to expand the total capacity output voltage. In addition, the electronic conductivity and lattice strain can be further boosted by nickel or cobalt substitutions. The benefits of this method are a more significant redox window, widening the cell voltage and an even spread of the lattice strain, lowering the volume change during cycling. (5)

Doping Ni or Co can generate more conductive pathways coupled with the capability to balance energy density, rate performance, and longevity by adjusting the ratio of different metals. However, this also comes with a challenge, such as the exacting mixing condition caused by the distinct ionic radius and bonding preference of each metal.The incomplete distribution can result in phase segregation and uneven performance and instability. A stable performance can be ensured through control over the precursor concentration, reaction rate, and temperature with the usage of advanced synthesis methods, such as controlled co-precipitation and hydrothermal growth or sol–gel processing.In the optimised state, the multi-metal PBA can provide a specific capacity level of approximately 120–150 mAh g−1 and operate stably over hundreds of charge–discharge cycles. This makes them excellent candidates for use in large-scale Na-ion ESS. (10)

2.6 Electrolytes, Interfaces, and Anode Counterparts

A battery's performance depends not only on its cathode but also on how efficiently ions and electrons move through the entire cell. Two key elements that influence this behaviour are the **electrolyte** and the **anode**. Together, they determine how reversible, safe, and stable the overall electrochemical process will be.

2.6.1 Electrolytes

Most sodium-ion batteries use **organic electrolytes** consisting of sodium salts such as $NaPF_6$, $NaClO_4$, or NaTFSI dissolved in carbonate-based solvents like ethylene carbonate (EC) and diethyl carbonate (DEC). These mixtures provide high ionic conductivity (on the order of 10^{-3} S cm^{-1}) and operate stably within a 0–4.5 V range.
Despite their effectiveness, organic electrolytes are **flammable** and sensitive to air and moisture. This has encouraged the development of safer alternatives:

- **Aqueous electrolytes** (for example, Na_2SO_4 or NaCl solutions) are inexpensive and non-flammable, though their limited voltage window (~1.2 V) reduces energy density.
- **Solid-state electrolytes** — including glassy, ceramic, or polymer conductors — offer excellent safety and thermal stability but suffer from higher interfacial resistance.
- **Additives** such as *fluoroethylene carbonate (FEC)* help stabilise the **solid–electrolyte interphase (SEI)** on anodes, reducing side reactions and improving cycle life.

The choice of electrolyte must ensure compatibility with both electrodes. A well-formed SEI layer is vital because it prevents continual electrolyte decomposition and preserves long-term battery efficiency. (11)

2.6.2 Anode Materials

On the anode side, graphite – the standard anode for LIBs – is an inappropriate host for Na^+, which is too large to fit in between the graphene layers. Therefore, the majority of SIB designs retain hard carbon as the anode material – a disordered form of non-graphitizable carbon that combines a certain number of graphitic planes with randomly located nanopores.Hard carbon accommodates Na on the surface via adsorption and intercalation in between the planes. It results in high reversible capacities of 250 – 300 mA h g −1, a working voltage of 0 – 2 V, and acceptable cycling stability. The main disadvantage of hard carbon involves relatively poor initial Coulombic efficiency – around 80 to 85%, due to SEI synthesis and the trapping of Na during the first charge.

Other potential anodes include
Alloy-type materials – Na–Sn, Na–Sb, Na–P. These compounds promise very high capacities while suffering from excessive volume change.

Conversion-type materials – metal oxides or sulfides that fully transform chemically and exhibit high theoretical capacity but poor reversibility. Thus, hard carbon remains the most efficient and cost-effective anode candidate for commercial SIBs. Combined with the aforementioned PBA cathode, hard carbon enables a reliable full-cell system for SIBs suitable for stationary and grid applications. (7)

2.7 Synthesis Strategies for PBA's

The synthesis method determines to a large extent the structure and performance of the Prussian Blue Analogues. The crystallisation process depends on a number of conditions, namely: All of these examples can be used for the synthesis of PBAs, although others may be too.

Co-Precipitation Method
The co-precipitation method involves the simultaneous reaction of metal salt precursors in an aqueous solution, leading to the rapid formation of Prussian Blue Analogues particles. This simple method involves combining aqueous solutions of transition-metal salts with alkali ferro- or ferricyanides. The resulting reaction forms a PBA precipitation that is insoluble and includes ageing, filtration, washing, and vacuum drying. Inexpensive, scalable, and co-precipitation is, however, characterised by the nonuniformity of particles. Also, there are a lot of empty states [Fe(CN) 6] 4 and unwanted structural liquid. Inexpensiveness and probing of each part of the precipitate can minimise defects by controlling concentration, stirring rate, and ageing time and support uniformity and crystallinity. (12)

Self-Decomposition Method
In the self-decomposition method, a metal–cyanide precursor slowly decomposes under controlled conditions to form Prussian Blue Analogues with improved crystallinity. The gradual reaction process allows better structural ordering and reduced defect formation. Here, a metal–cyanide complex such as $Na_4[Fe(CN)_6]$ slowly decomposes in solution, releasing Fe^{2+} or Fe^{3+} that reacts with other metal ions (e.g., Mn^{2+}). The slower reaction rate produces more ordered crystals with fewer defects and better electronic conductivity. Drying is typically done at 120–150 °C under vacuum. The trade-off is longer synthesis time and lower throughput, though the structural quality is superior. (12)

Hydrothermal Method
The hydrothermal method involves synthesizing Prussian Blue Analogues in a sealed autoclave under elevated temperature and pressure, promoting controlled crystal growth to about 100–160 °C. The elevated temperature and pressure allow precise control of nucleation and particle growth, yielding uniform nanostructures such as cubes or spheres. These small, well-crystallised particles offer short Na^+ diffusion paths and high rate capability. The downside is higher cost and limited scalability. (12)

Method	Advantages	Limitations
Co-precipitation	Simple, scalable, inexpensive	High defect level; poor size control
Self-decomposition	High crystallinity; few vacancies	Long reaction time; limited scale-up
Hydrothermal	Uniform morphology; tunable shape	Costly; energy-intensive

Table 2- Comparison of PBA synthesis methods and their trade-offs.

To combine the strengths of each, researchers are experimenting with **hybrid routes**, such as slow co-precipitation followed by mild hydrothermal treatment. Post-synthesis steps like **vacuum drying**, **carbon coating**, and **surface passivation** further enhance conductivity and moisture resistance.

3 METHODLOGY

3.1 Overview

This chapter describes the experimental procedures used to create and characterise multi-metal PBA's (PBAs) as possible cathode materials for sodium-ion batteries. The primary goal of this research was to find a synthesis technique that is efficient, repeatable, and capable of creating PBAs with high crystallinity, low defect concentration, and stable electrochemical performance. To accomplish this, three synthesis approaches—co-precipitation, self-decomposition, and hydrothermal methods—were thoroughly studied, with all pathways using identical precursor materials, stoichiometry, and post-synthesis treatment processes to assure a fair comparison. Following synthesis, the prepared multi-metal PBAs were thoroughly characterised using a variety of structural, morphological, thermal, and electrochemical techniques, including X-ray diffraction (XRD), scanning electron microscopy (SEM), cyclic voltammetry (CV), and galvanostatic charge-discharge (GCD) testing.

3.2 Research Design and Approach

The research study took a comparative perspective with respect to understanding how distinct synthesis methods alter the structural, morphological, and electrochemical aspects. Each synthesis method was chosen for different reasons: (1) The co-precipitation method is easy and scalable, but results in defects that are associated with either water or vacancies. (2) The self-decomposition method allows for slow crystal growth, which enhances the structural quality. (3) The hydrothermal method is valuable because it can regulate particle morphology by using temperature and pressure.With three samples made from the same chemical composition, the research sought information on how synthesis conditions were able to influence layers of Na^+-storage capacity, cycling stability, and overall battery performance.This approach allows for valid comparisons of each method, as well as determining the best route for large-scale and sustainable production.

3.3 Materials and Chemicals

All reagents were **analytical grade** and used as received without further purification. The main precursors included:

Sl. No.	Chemical Name	Chemical Formula	Metal Source(s)	Function / Purpose
1	**Iron(II) chloride tetrahydrate**	**$FeCl_2 \cdot 4H_2O$**	**Fe^{2+}**	Primary Fe^{2+} precursor for the PBA lattice formation
2	**Manganese(II) chloride tetrahydrate**	**$MnCl_2 \cdot 4H_2O$**	**Mn^{2+}**	Mn precursor introducing redox-active Mn sites
3	**Cobalt(II) chloride hexahydrate**	**$CoCl_2 \cdot 6H_2O$**	**Co^{2+}**	Co precursor improving electronic conductivity and stability
4	**Copper(II) chloride dihydrate**	**$CuCl_2 \cdot 2H_2O$**	**Cu^{2+}**	Cu source enhancing mixed-valence redox behaviour
5	**Nickel(II) chloride hexahydrate**	**$NiCl_2 \cdot 6H_2O$**	**Ni^{2+}**	Ni precursor contributing to lattice stability and structural integrity
6	**Sodium hexacyanoferrate(II) decahydrate**	**$Na_4[Fe(CN)_6] \cdot 10H_2O$**	**$[Fe(CN)_6]^{4-}$**	Cyanometallate complex forming the PBA framework with Fe^{2+} centers
7	**Sodium hexacyanoferrate(III)**	**$Na_3[Fe(CN)_6]$**	**$[Fe(CN)_6]^{3-}$**	Mixed-valence cyanometallate source aiding charge balance and structural rigidity
8	**Deionized (DI) water**	–	–	Solvent and medium for precursor dissolution and reaction
9	**Ethanol (washing solvent)**	**C_2H_5OH**	–	Used for washing and removing surface impurities after filtration

Table 3 - Chemicals Used for the Synthesis of Fe–Mn–Co–Cu–Ni Multi-Metal PBA's (PBAs)

All experiments were carried out in a fume hood while wearing protective gloves, a lab coat, and safety goggles.

3.4 Experimental Synthesis Procedures

Three distinct routes were employed to synthesise the multi-metal PBAs, each using the same metal ratio and target stoichiometry:

$$A_x M_1[M_2(CN)_6]_{1-y} \cdot nH_2O$$

where A = Na^+, M_1 and M_2 = Fe, Mn, Ni (multi-metal composition).

3.4.1 Co-Precipitation Method

1. **Solution preparation:** Separate aqueous solutions of $FeCl_3 \cdot 6H_2O$, $MnCl_2 \cdot 4H_2O$, $CoCl_2 \cdot 6H_2O$, $CuCl_2 \cdot 2H_2O$ and $NiCl_2 \cdot 6H_2O$ were prepared (0.1 M each).
2. **Reaction:** The mixed metal solution was slowly added dropwise into a 0.05 M $Na_4[Fe(CN)_6]$ solution under constant stirring at room temperature (≈ 25 °C).
3. **Ageing:** The mixture was allowed to stand undisturbed for **48 hours** to complete precipitation and crystal growth.
4. **Washing:** The precipitate was filtered and repeatedly washed with deionised water and ethanol to remove unreacted ions.
5. **Drying:** The product was dried in a **vacuum oven at 100 °C for 8 hours**, producing a fine blue powder.

The resulting sample, labelled **PBA-CP**, was stored in airtight containers to prevent moisture absorption.

3.4.2 Self-Decomposition Method

1. **Precursor formation:** A 0.05 M solution of $Na_4[Fe(CN)_6]$ was prepared in deionized water.
2. **Decomposition reaction:** The solution was left to decompose slowly at ambient temperature for 24 hours, releasing Fe^{2+}/Fe^{3+} ions.
3. **Metal addition:** A mixed metal solution ($FeCl_3$, $CoCl_2$, $CuCl_2$, $NiCl_2$ and $MnCl_2$ in equal molar ratio) was added dropwise to the decomposing mixture.
4. **Ageing and washing:** The suspension was aged for 48 hours to ensure homogeneous reaction, then washed several times with DI water and ethanol.
5. **Drying:** The sample was vacuum-dried at **150 °C for 8 hours**, resulting in a highly crystalline powder.

This product, **PBA-SD**, was expected to show lower vacancy concentration and better phase purity due to its slower formation rate.

3.4.3 Hydrothermal Method

1. **Solution mixing:** 0.1 M $FeCl_3 \cdot 6H_2O$ and 0.1 M $Na_4[Fe(CN)_6]$ were mixed in 50 mL of DI water.
2. **pH adjustment:** The solution was adjusted to **pH ≈ 6.5** using dilute NaOH to control crystal nucleation.
3. **Sealing and heating:** The mixture was transferred to a **Teflon-lined autoclave**, sealed, and heated to **150 °C for 10 hours**.
4. **Cooling and collection:** After natural cooling to room temperature, the precipitate was collected, washed, and dried at **60°C for 6 hours**.

The obtained sample, **PBA-HT**, displayed uniform morphology and good crystallinity. All three samples were synthesised using identical Na^+ stoichiometry and metal ratios, ensuring that differences in performance could be attributed primarily to synthesis technique.

3.5 Electrode Preparation

The synthesised powders were used as the **active material** for cathode fabrication. Each cathode film was prepared using the following steps:

1. **Slurry mixing:** The active material, conductive carbon black, and polyvinylidene fluoride (PVDF) binder were combined in an **8:1:1 weight ratio**.
2. **Solvent addition:** N-methyl-2-pyrrolidone (NMP) was added as a solvent, and the mixture was stirred until a uniform slurry formed.
3. **Coating:** The slurry was uniformly coated onto carbon-coated aluminium **foil** (current collector) using a doctor-blade applicator.
4. **Drying:** Coated electrodes were dried in a vacuum oven at **100 °C for 12 hours** to remove residual NMP.
5. **Cutting and pressing:** Dried electrodes were pressed and cut into circular discs (12 mm diameter) for cell assembly.

The final electrode loading was approximately **1.8 mg cm^{-2}** of active material.

3.6 Coin-Cell Assembly

Electrochemical testing was performed using CR2032 coin cells, assembled in an argon-filled glove box where both oxygen and moisture levels were maintained below 0.1 ppm.

The cell components included:

- **Cathode:** the prepared PBA film on aluminium foil.

- **Anode:** high-purity sodium metal foil (counter/reference electrode).
- **Separator:** glass-fibre filter paper.
- **Electrolyte:** 1 M $NaPF_6$ dissolved in a 1:1 volume ratio of EC and DEC.

After assembly, the cells were crimped tightly to prevent electrolyte leakage. All electrochemical tests were carried out at room temperature (25 ± 2 °C).

3.7 Material Characterisation

A combination of structural, morphological, and thermal analyses was conducted to confirm the successful synthesis and quality of PBAs.

- **X-ray Diffraction (XRD):** X-ray diffraction (XRD) is used to determine the crystal structure, phase purity, and crystallinity of manufactured PBA powders. When X-rays (Cu-Kα, λ = 1.5406 Å) contact a crystalline material, they are diffracted by its regularly spaced atomic planes. Constructive diffraction happens when the Bragg condition is met, which is represented by $n\lambda = 2d \sin\theta$, where d is the interplanar distance and θ is the diffraction angle. Recording intensity as a function of 2θ (often 10-80°) creates a unique "fingerprint" pattern. Sharp and well-defined peaks in PBAs often imply high crystallinity and an ordered cubic framework, whereas broad peaks may suggest tiny crystallite size, low crystallinity, or flaws. Peak positions can be utilized to confirm the predicted PBA phase by comparing to conventional reference patterns; any additional peaks may indicate contaminants or secondary phases. Furthermore, lattice parameters can be calculated from peak positions (particularly if the material is cubic), and relative variations in lattice constant may indicate metal replacement, sodium content variation, or water/vacancy concentration inside the framework.
- **Scanning Electron Microscopy (SEM):** Scanning Electron Microscopy (SEM) produces high-resolution pictures of the sample surface and is used to assess particle shape, size, distribution, and agglomeration of PBAs. SEM operates by scanning a concentrated electron beam across the sample surface. Secondary electrons are generated as a result of interactions between the beam and the sample, and these signals are collected to build a comprehensive topographical image. SEM is particularly beneficial for PBAs since the synthesis processes have a substantial influence on the resulting microstructure—for example, co-precipitation frequently creates more agglomerated particles, whereas hydrothermal procedures can produce more uniform, well-defined crystals. SEM pictures can provide information such as cubic particle shape, surface smoothness/roughness, particle size range (e.g., 200-500 nm), and degree of clustering, all of which are important for electrochemical activity. Smaller and more uniform particles shorten sodium-ion diffusion routes and may increase rate capability, but severe agglomeration restricts electrolyte access and reduces effective active surface area.

- **Energy-Dispersive X-ray Spectroscopy (EDS):** Energy-Dispersive X-ray Spectroscopy (EDS) is often used in conjunction with SEM to identify elemental composition and spatial distribution of elements within a sample. When the SEM electron beam strikes the sample, it can eject inner-shell electrons from the atoms. When higher-energy electrons fall back to fill these vacancies, the material emits X-rays with element-specific energies. By measuring these energies, EDS can determine which elements are present and provide estimated elemental ratios. EDS is used in PBAs to confirm the successful inclusion of selected metals (such as Fe, Mn, Co, Cu, and Ni) and to ensure that the composition is uniform throughout the sample. Elemental mapping is especially crucial for multi-metal PBAs since it helps to ensure that metals are evenly dispersed rather than divided into distinct regions or phases. While EDS is effective at confirming the existence and distribution of heavy elements, it is less accurate for light elements and cannot accurately quantify components such as hydrogen; thus, it is frequently used in conjunction with XRD/FTIR and other techniques. Also, sodium might be difficult to measure depending on instrument settings, so it's best to record it as "detected" and use mapping trends rather than claiming exact stoichiometry.
- **Fourier-Transform Infrared Spectroscopy (FT-IR):** Fourier-Transform Infrared Spectroscopy (FT-IR) is utilized to confirm chemical bonding and functional groups in synthesized PBAs, namely the cyanide linkage that forms the framework. FT-IR detects how a sample absorbs infrared light at various wavenumbers; absorption peaks correspond to the vibrational modes of individual bonds. The main characteristic of PBAs is the C≡N stretching vibration, which typically appears as a strong band in the ~2000-2200 cm^{-1} range. The exact position and shape of this band vary depending on the metals' oxidation state, the metal-cyanide bonding environment, and defect/water concentration. FT-IR can also detect bands associated with metal-N or metal-C interactions (typically at lower wavenumbers), as well as O-H stretching/bending bands associated with adsorbed or coordinated water, which lends validity to your explanation of hydration and stability. Overall, FT-IR is complementary to XRD: XRD validates the crystalline phase and lattice order, whereas FT-IR confirms the chemical formation of the cyanide-bridged coordination framework and can provide indirect information regarding bonding strength and hydration.
- These characterisation techniques provided the foundation for interpreting the electrochemical results discussed in later chapters.

3.8 Electrochemical Characterisation

The electrochemical properties of the synthesised PBAs were evaluated through three main tests: galvanostatic charge–discharge (GCD), cyclic voltammetry (CV), and electrochemical impedance spectroscopy (EIS).

3.8.1 Cyclic Voltammetry (CV)

CV measurements were conducted between 2.0–4.0 V at a scan rate of 0.1 mV s^{-1}. The position and area of redox peaks indicated the reversibility and kinetics of Na^+ insertion/extraction processes. Overlapping curves in consecutive cycles confirmed electrochemical stability.

3.8.2 Electrochemical Impedance Spectroscopy (EIS)

EIS was measured over the frequency range of 0.01 Hz to 100 kHz with an amplitude of 5 mV. Nyquist plots were used to extract charge-transfer resistance (Rct) and Warburg impedance, which reflect ion-diffusion behaviour in the electrode.
Comparing EIS data among PBA-CP, PBA-SD, and PBA-HT samples allowed direct evaluation of which synthesis route provided better electronic and ionic conductivity.

3.9 Data Analysis and Comparison

All experimental measurements were performed **in triplicate** to ensure reproducibility. Results from each synthesis route were analysed based on:

- **Crystallinity:** determined from XRD peak intensity and sharpness.
- **Particle morphology:** from SEM and EDS imaging.
- **Electrochemical performance:** from GCD and CV curves, including capacity, efficiency, and rate capability.

Performance metrics such as **specific capacity**, **Coulombic efficiency**, and **capacity retention** were plotted against cycle number. This comparative approach made it possible to identify correlations between synthesis conditions and electrochemical behaviour.

4 RESULTS AND DISCUSSION

4.1 Co-Precipitation Method

4.1.1 Structural Characterisation (XRD Analysis)

The co-precipitation route yielded a poly-metallic Prussian Blue Analogues containing Fe, Mn, Co, Cu, and Ni within a single cubic framework. The X-ray diffraction pattern (ICDD: 01-080-2395) confirmed the formation of a face-centred cubic (Fm-3m) structure typical of PBAs. The reflections observed at approximately 17.5°, 24.8°, 35.3°, 39.7°, 43.5°, and 50.6° (2θ) correspond to the (200), (220), (400), (420), (422), and (440) planes, matching the standard PBA phase without any impurity peaks. The close alignment of the experimental and reference peaks indicates successful incorporation of multiple transition-metal species into a single lattice rather than formation of separate phases. However, the broadening of peaks and the moderate background intensity suggest smaller crystallite domains and partial lattice strain, both expected consequences of rapid ionic precipitation during multi-metal mixing. The substitution of several transition metals into the Fe–C≡N–M network likely introduced micro-strain due to differences in ionic radii and coordination environments.

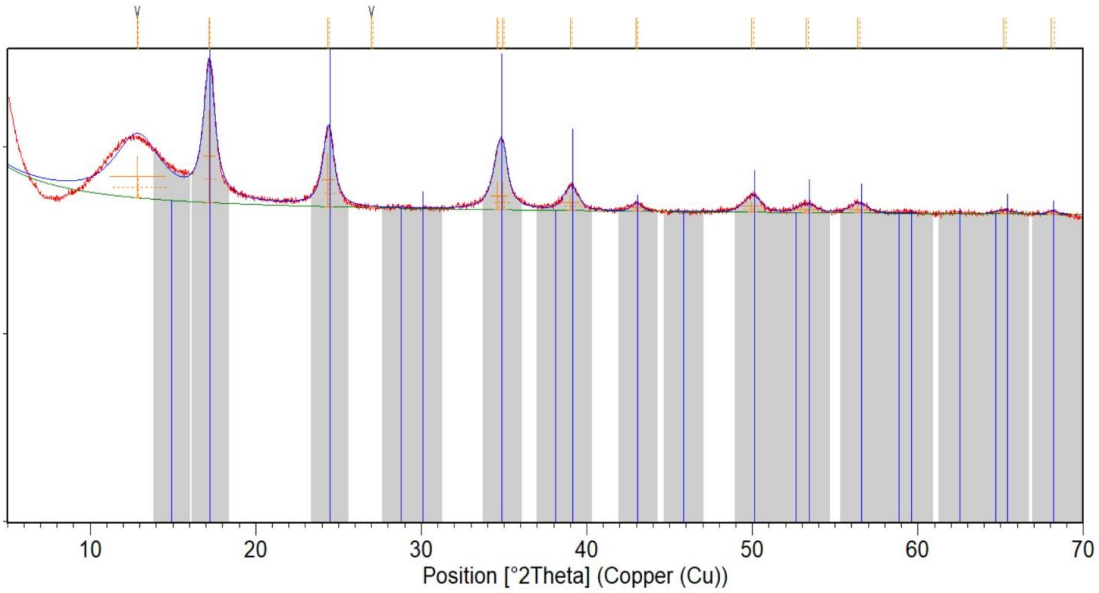

Figure 3- X-ray diffraction (XRD) pattern of the Fe–Mn–Co–Cu–Ni PBA synthesised via the Co-precipitation route showing characteristic cubic reflections corresponding to the Fm-3m phase (ICDD: 01-080-2395)

4.1.2 Morphological Analysis (SEM Observations)

The SEM micrographs (Figure 3) show that the co-precipitated product consists mainly of large, irregular polyhedral blocks surrounded by fine fragments. At lower magnification, the surface appears rough with multiple cracks and loosely bound particles, while higher-magnification images reveal a layered texture across the facets, implying partial agglomeration of smaller crystallites. The particle size varies widely from sub-micron fragments to agglomerates exceeding several micrometres. Such heterogeneity is typical of fast precipitation processes where multiple cations compete for coordination sites, leading to uneven nucleation rates. The absence of well-defined cubic particles and the presence of coarse aggregates indicate limited control over crystal growth. This morphology, although characteristic of as-prepared PBAs, can

restrict the accessibility of Na^+ diffusion channels and lower the active surface area, potentially affecting electrochemical performance.

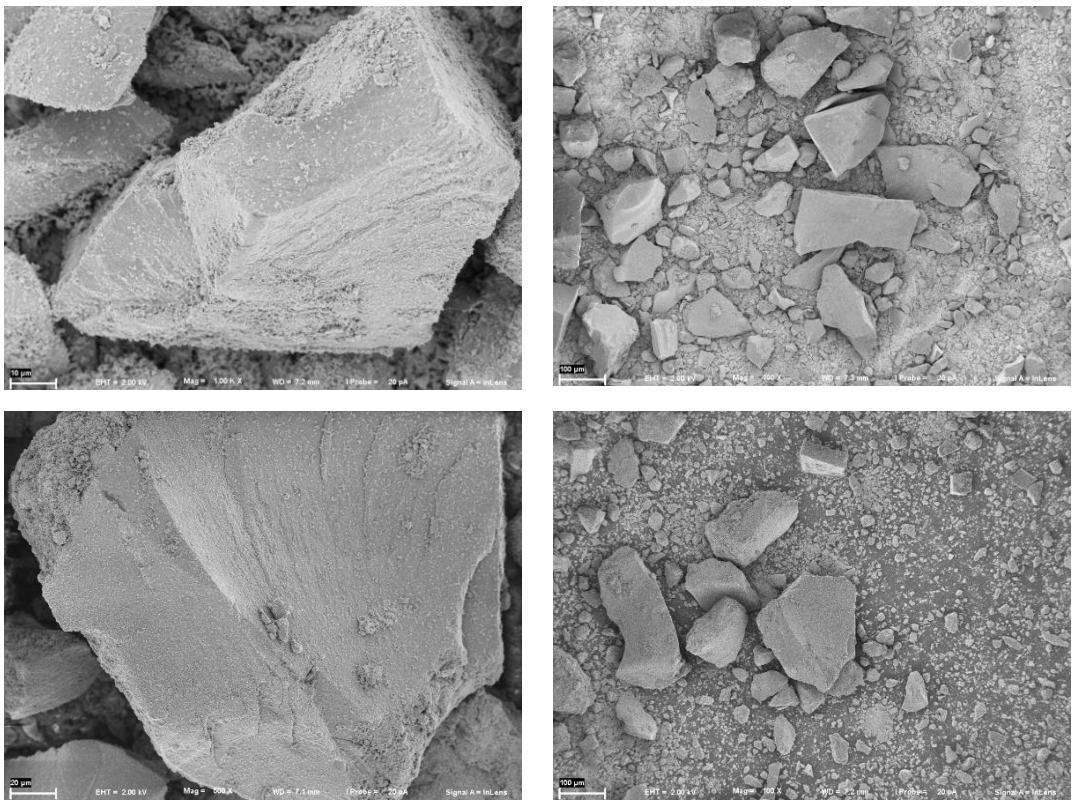

Figure 4 - Scanning electron microscopy (SEM) micrographs of co-precipitated Fe–Mn–Co–Cu–Ni PBA showing irregularly shaped particles with broader size distribution and noticeable agglomeration.

4.1.3 Electrochemical Characterisation (CV and GCD Results)

The electrochemical behaviour, illustrated by cyclic-voltammetry (CV) and galvanostatic charge–discharge (GCD) profiles (Figure 4.2), further clarifies the impact of structural features on performance. The CV curves displayed two broad redox couples centred at approximately 3.1 V and 3.4 V, corresponding to the Fe^{2+}/Fe^{3+} and mixed Mn^{2+}/Mn^{3+}–Co^{2+}/Co^{3+} transitions. The peaks were stable over successive cycles, confirming reversible Na^+ intercalation/deintercalation; however, the evident peak broadening and separation indicate moderate polarisation and slower redox kinetics. The GCD curves exhibited a stable voltage plateau in the range of 3.2–3.4 V, characteristic of the PBA structure, with an initial specific capacity of about 80 mAh g^{-1}. Capacity retention was steady across multiple cycles, but the sloping discharge segment following the plateau suggested partial pseudocapacitive behaviour from surface sites and defects. Overall, the electrochemical response of the co-precipitated Fe–Mn–Co–Cu–Ni PBA demonstrates that, while the structure enables sodium storage, internal lattice imperfections and morphological irregularities limit ion transport and energy efficiency.

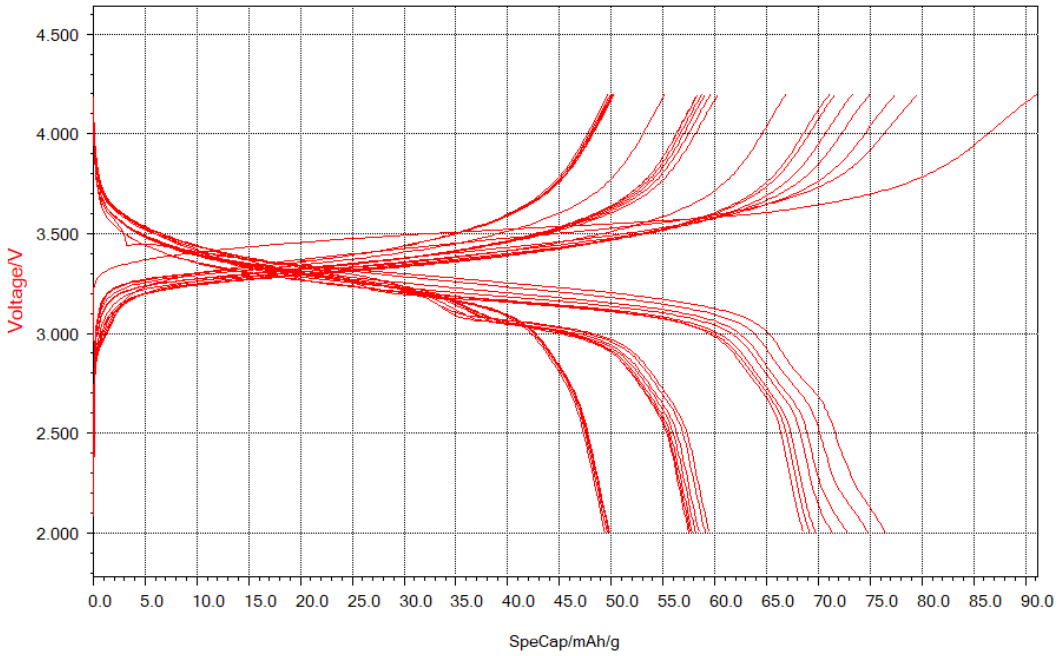

Figure 5 - Electrochemical performance of the Co-precipitated Fe–Mn–Co–Cu–Ni PBA: Galvanostatic charge–discharge (GCD) profile displaying voltage plateaus between 3.2–3.4 V.

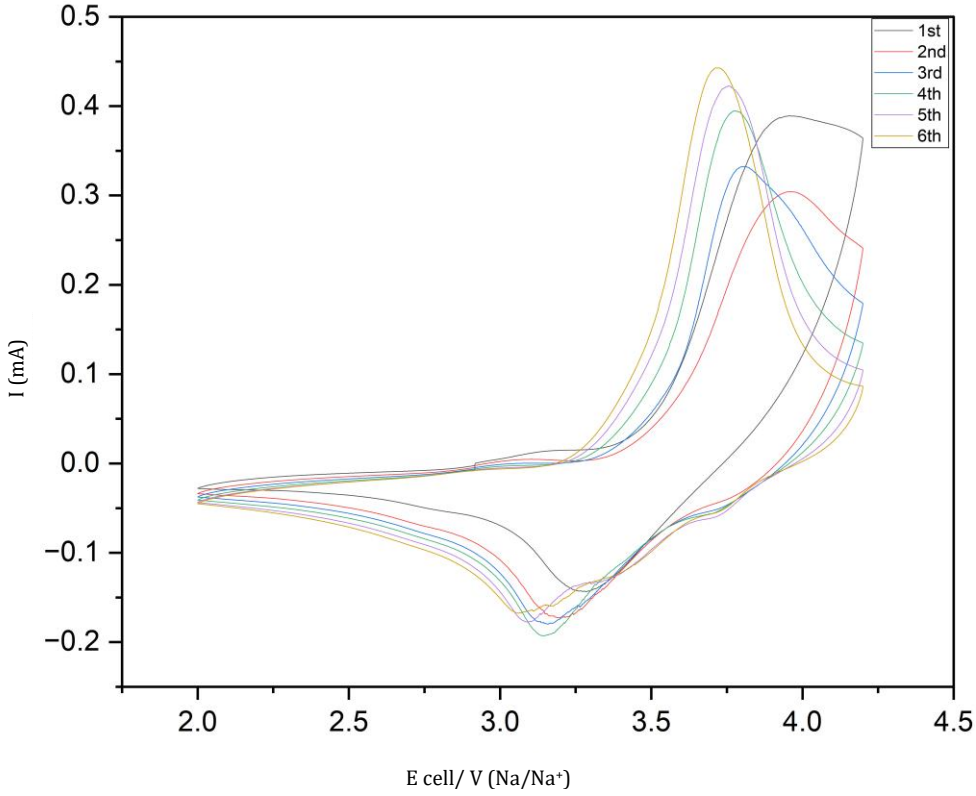

Figure 6- Cyclic-voltammetry (CV) curve showing Fe^{2+}/Fe^{3+} and Mn^{2+}/Mn^{3+}–Co^{2+}/Co^{3+} redox peaks

4.2 Self-Decomposition Method

4.2.1 Structural Characterisation (XRD Analysis)

The self-decomposition method yielded a uniformly crystalline and phase-pure multi-metal Prussian Blue Analogues containing Fe, Mn, Co, Cu, and Ni, with a distinctly ordered cubic morphology. The X-ray diffraction pattern (ICDD reference 01-083-2293) confirmed the formation of a face-centred cubic lattice (Fm-3m) characteristic of PBAs. Prominent diffraction peaks appeared at approximately 17.5°, 24.8°, 35.3°, 39.7°, 43.5°, and 50.6° (2θ), indexed to the (200), (220), (400), (420), and (440) planes of the Prussian Blue structure. These peaks were sharper and more intense compared to those obtained from the co-precipitated sample, signifying higher crystallinity and a more ordered framework. The absence of impurity reflections confirmed the successful formation of a single phase, despite the presence of multiple transition metals. The narrow full-width at half maximum (FWHM) of the peaks reflects uniform crystal growth and minimal lattice strain, suggesting that the slower ion-release rate during the self-decomposition process facilitated homogeneous incorporation of Fe, Mn, Co, Cu, and Ni into the lattice. The close match with the reference pattern demonstrates that the PBA structure remained stable during decomposition and no secondary metal cyanide phases were formed.

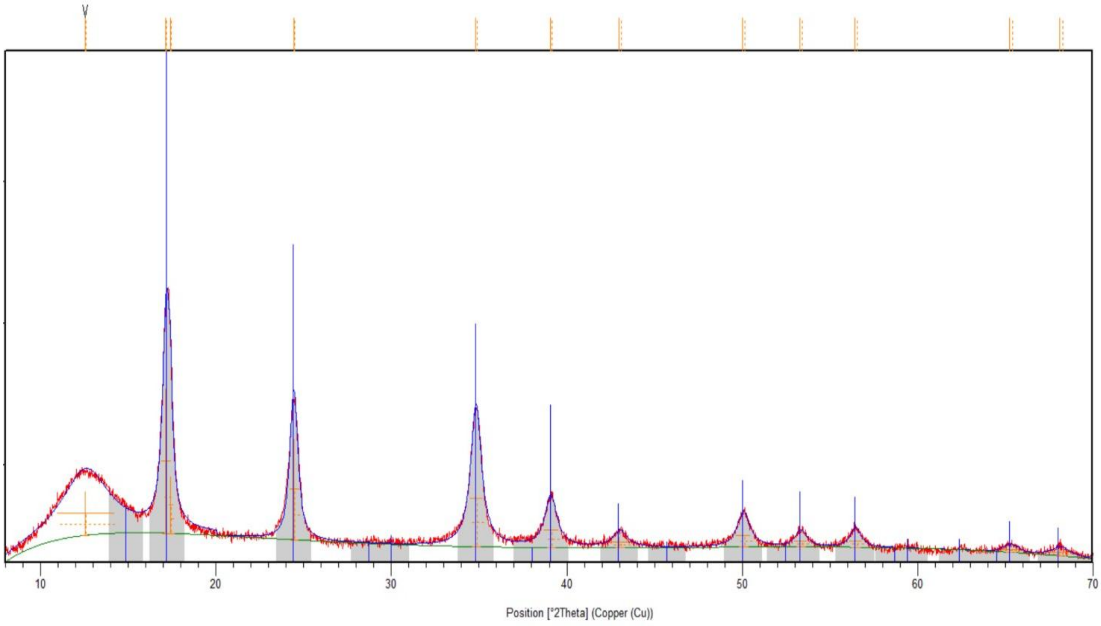

Figure 7- X-ray diffraction (XRD) pattern of the Fe–Mn–Co–Cu–Ni PBA synthesised via the self-decomposition route, confirming a highly crystalline Fm-3m cubic structure (ICDD: 01-083-2293).

4.2.2 Morphological Analysis (SEM Observations)

SEM micrographs of the self-decomposed sample (Figure 4.3) clearly display well-defined cubic crystals with smooth facets and sharp edges, distributed uniformly across the surface. Particle sizes were predominantly in the range of 200–500 nm, smaller and more uniform than those of the co-precipitated sample. At higher magnification, the cubes appeared slightly covered with fine nanoparticles, possibly representing secondary nucleation or small crystallites adhering to the main cubes.
The particles were evenly dispersed with minimal aggregation, indicating that the slow decomposition and controlled ion diffusion during synthesis ensured gradual and orderly crystal growth. The uniform cubic morphology with smooth surfaces enhances particle–particle contact and shortens Na^+ ion-diffusion paths, leading to improved electrochemical kinetics. The high degree of shape regularity also implies reduced defect density and fewer $[Fe(CN)_6]$ vacancies within the framework.

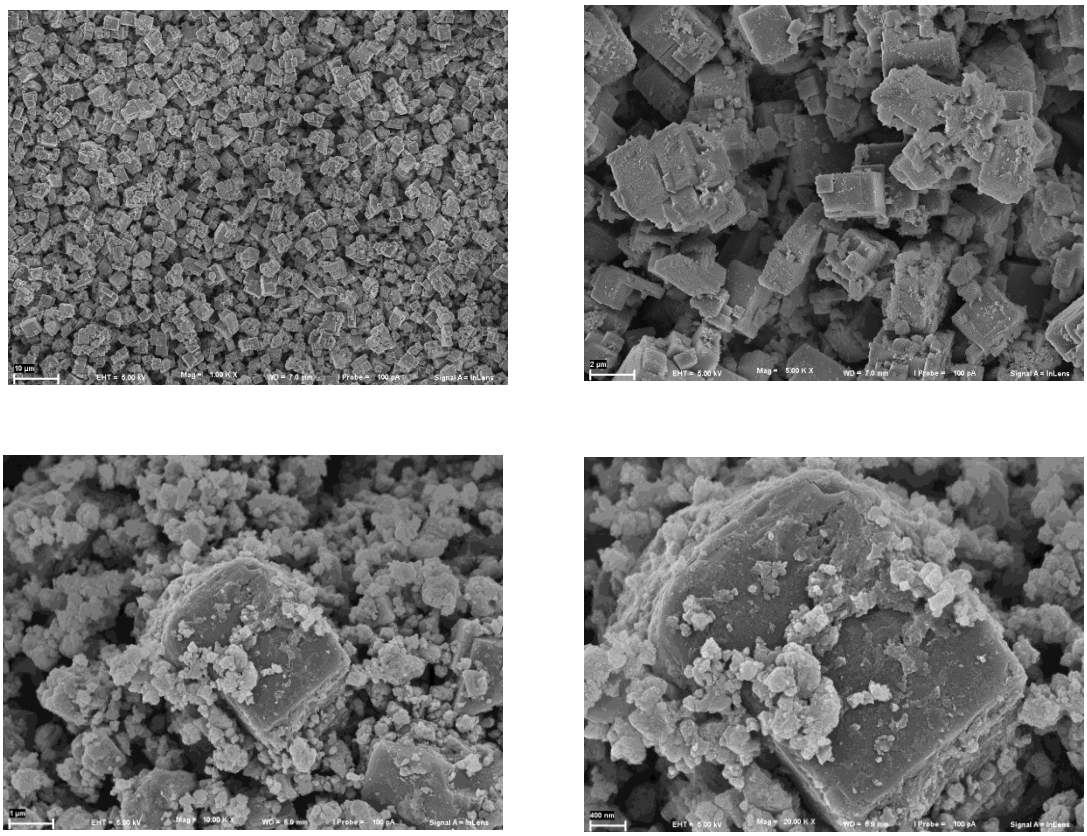

Figure 8- Scanning electron microscopy (SEM) micrographs of the Self-decomposed Fe–Mn–Co–Cu–Ni PBA showing uniform cubic crystals (200–500 nm) with smooth surfaces and minimal agglomeration.

4.2.3 Electrochemical Performance (CV and GCD Results)

Electrochemical measurements confirmed the superior reversibility and conductivity of this material. The cyclic-voltammetry (CV) profiles (Figure 4.4, right) exhibited two distinct and symmetric redox peaks at around 3.1 V and 3.4 V, corresponding to the Fe^{2+}/Fe^{3+} and mixed Mn^{2+}/Mn^{3+}–Co^{2+}/Co^{3+} transitions. The near overlap of the oxidation and reduction peaks across successive cycles indicated excellent reversibility and stability of the redox reactions. The galvanostatic charge–discharge (GCD) curves (Figure 4.4, left) displayed flat and consistent voltage plateaus between 3.2 and 3.4 V, confirming the intercalation–deintercalation mechanism typical of PBA cathodes. The initial specific capacity reached approximately 100 mAh g^{-1}, with minimal fading over repeated cycles, demonstrating high structural stability. Compared with the co-precipitated sample, the polarisation voltage gap was smaller, and the charge–discharge profiles were more symmetric, indicating faster Na^+ kinetics and lower internal resistance. The overall electrochemical behaviour suggests that the self-decomposition process produced the most homogeneous and efficient multi-metal PBA structure among all the synthesis routes investigated.

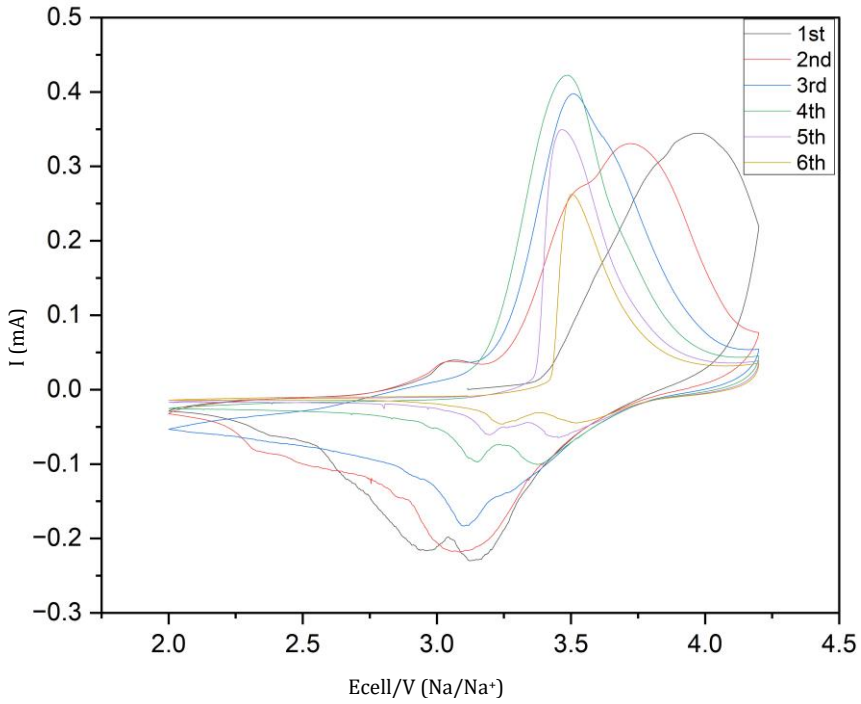

Figure 9- Electrochemical characteristics of the Self-decomposed Fe–Mn–Co–Cu–Ni PBA: Cyclic-voltammetry (CV) profile showing sharp and symmetric redox peaks near 3.1 and 3.4 V

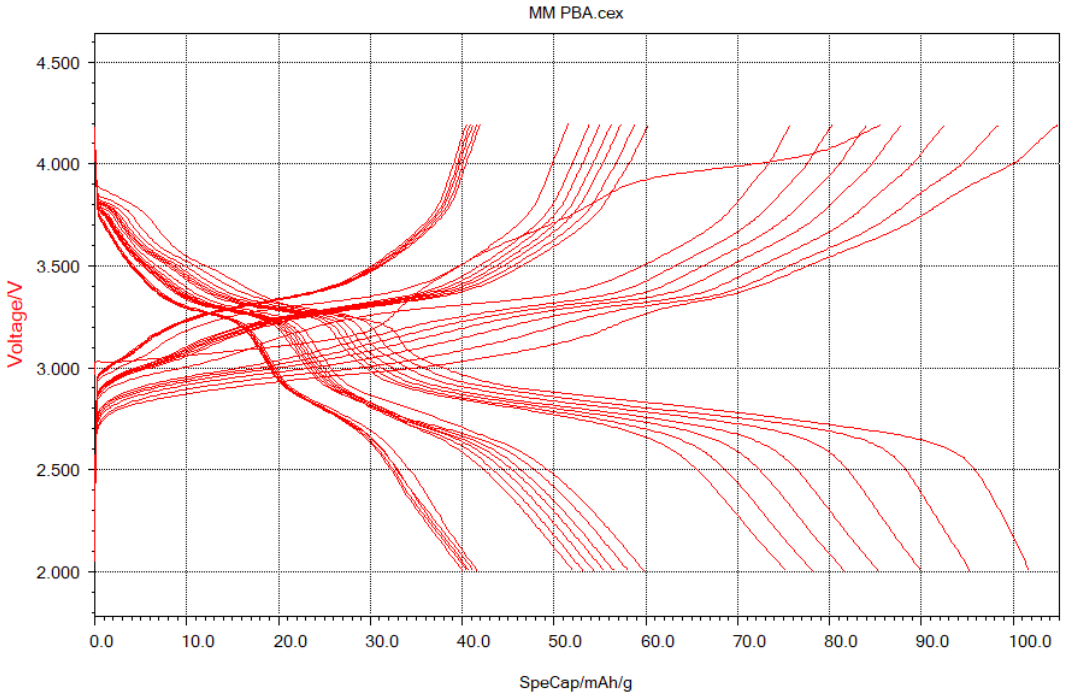

Figure 10- Electrochemical characteristics of the Self-decomposed Fe–Mn–Co–Cu–Ni PBA: Galvanostatic charge–discharge (GCD) curve exhibiting stable plateaus and high

4.3 Hydrothermal Method

4.3.1 Structural Characterisation (XRD Analysis)

The hydrothermal method successfully produced a multi-metal Prussian Blue Analogues (PBA) containing Fe, Mn, Co, Cu, and Ni within a single cubic framework. The X-ray diffraction (XRD) pattern, indexed to ICDD reference 01-086-0502, confirmed the presence of the face-centred cubic (Fm-3m) phase typical of PBAs. Distinct diffraction peaks were observed at approximately 17.5°, 24.8°, 35.3°, 39.7°, 43.5°, and 50.6° (2θ), corresponding to the (200), (220), (400), (420), and (440) planes. The sharpness of the reflections verified a well-crystallised structure; however, the relative intensities of the peaks were slightly lower than those of the self-decomposed sample, indicating moderate crystallinity and possible micro-strain within the lattice. The absence of any impurity reflections suggests that the hydrothermal reaction conditions (120 °C, 10 h) enabled homogeneous incorporation of all transition metals without formation of separate oxide or cyanide phases. The minor peak broadening could be attributed to residual stress or partial disorder induced by the coexistence of multiple cations with different ionic radii and coordination preferences.

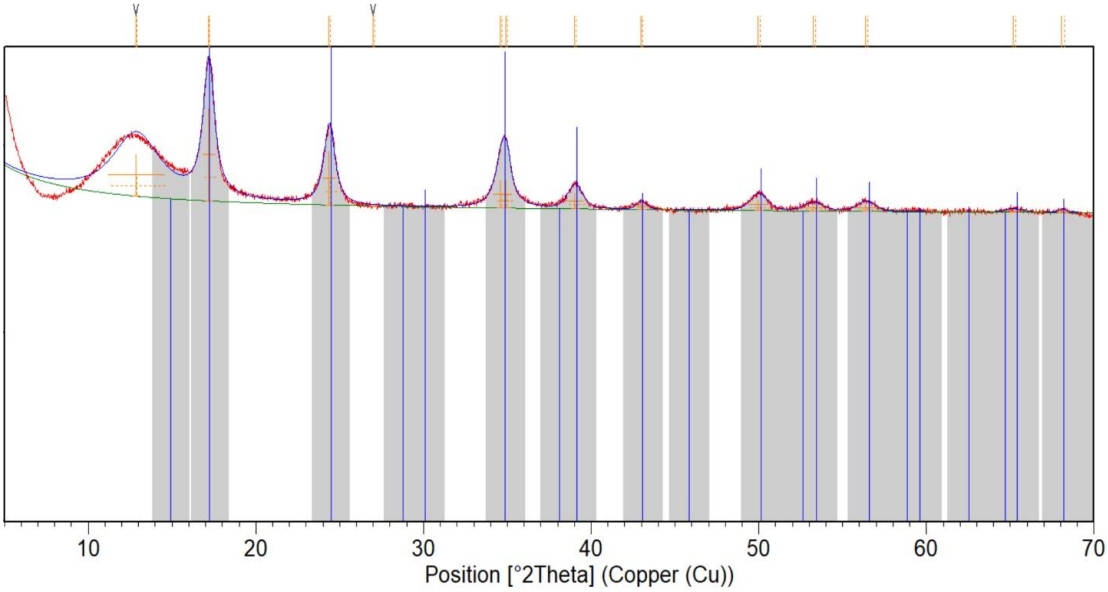

Figure 11- X-ray diffraction (XRD) pattern of the Fe–Mn–Co–Cu–Ni PBA synthesised via the hydrothermal route, indicating phase-pure cubic structure (ICDD: 01-086-0502) with moderate crystallinity.

4.3.2 Structural Characterisation (XRD Analysis)

The SEM micrographs (Figure 4.5) showed that the hydrothermally synthesised PBA comprised spherical-to-polyhedral nanoparticles distributed uniformly across the surface. The particle size was notably smaller compared with the co-precipitated sample, generally ranging from 100 to 300 nm, with many agglomerates visible due to particle coalescence during thermal treatment. The morphology revealed the coexistence of smooth and angular grains, suggesting that nucleation and growth occurred concurrently under the high-pressure conditions of the autoclave. The particles were densely packed, and small nanocrystallites appeared to adhere to the surfaces of larger grains, likely formed through secondary nucleation during cooling. The overall morphology indicates partial aggregation but good uniformity, a common characteristic of hydrothermal PBAs, where elevated temperature enhances diffusion and promotes isotropic growth. The combination of small particle size and high surface area can enhance electrolyte contact and improve ion-exchange kinetics, though excessive porosity may also trap water molecules within the structure.

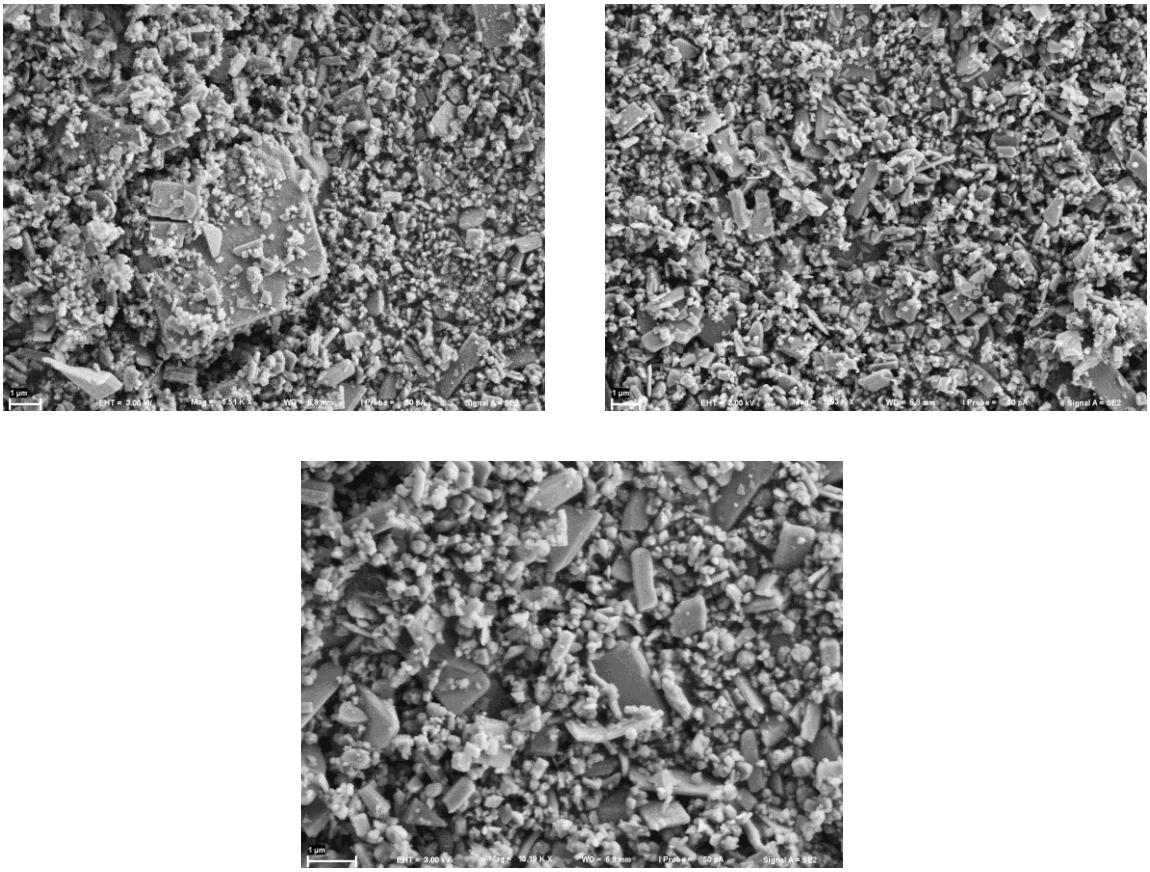

Figure 12 - Scanning electron microscopy (SEM) micrographs of the Hydrothermally synthesised Fe–Mn–Co–Cu–Ni PBA depicting spherical-to-polyhedral nanoparticles (100–300 nm) with partial agglomeration.

4.3.3 Electrochemical Characterisation (CV and GCD Results)

The electrochemical performance of the hydrothermally synthesised sample reflected these structural and morphological characteristics. The cyclic-voltammetry (CV) profiles (Figure 4.6, right) exhibited distinct and symmetric redox peaks at around 3.1 V and 3.4 V, associated with the Fe^{2+}/Fe^{3+} and mixed Mn^{2+}/Mn^{3+}–Co^{2+}/Co^{3+} couples. The peak separation was slightly larger than that of the self-decomposed sample, suggesting moderate polarisation and slower charge-transfer kinetics. The galvanostatic charge–discharge (GCD) curves (Figure 4.6, left) displayed stable and well-defined voltage plateaus between 3.2 V and 3.4 V, indicative of reversible Na^+ intercalation within the PBA lattice. The initial specific capacity reached approximately 85 mAh g^{-1}, maintaining good capacity retention across multiple cycles. Although slightly lower than that of the self-decomposition sample, the relatively flat voltage profiles confirm efficient multi-electron redox activity contributed by all transition metals. The stable cycling behaviour and consistent CV overlap suggest that the hydrothermally synthesised PBA maintained good structural integrity throughout electrochemical cycling.

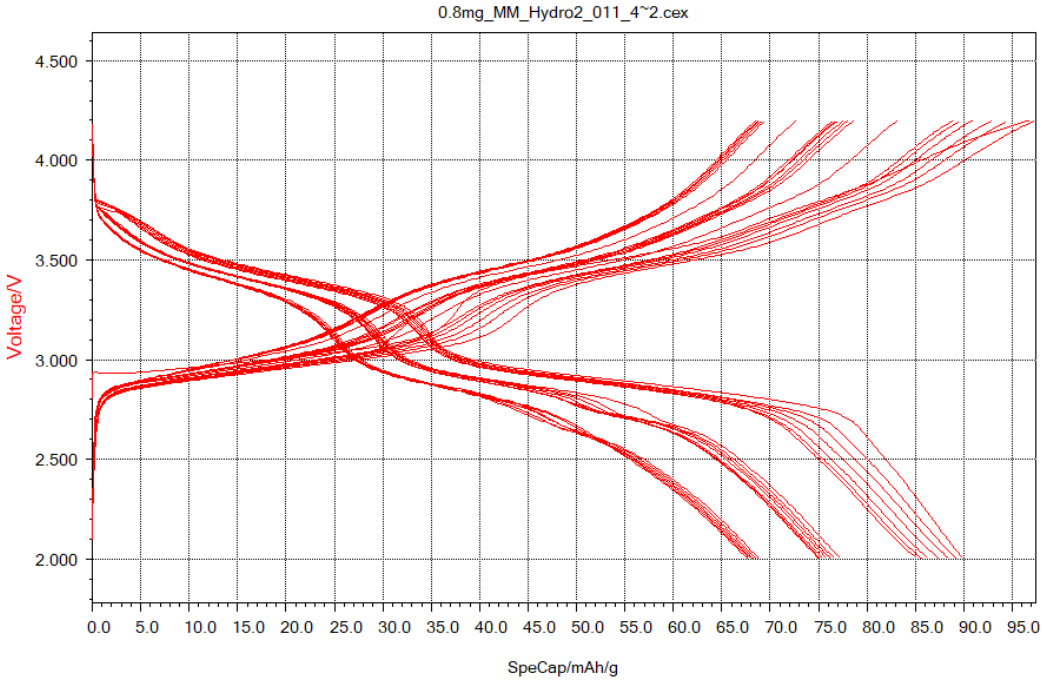

Figure 13 - Electrochemical results of the Hydrothermal Fe–Mn–Co–Cu–Ni PBA Galvanostatic charge–discharge (GCD) curve showing moderate capacity (~90 mAh g^{-1}) and stable cycling behaviour.

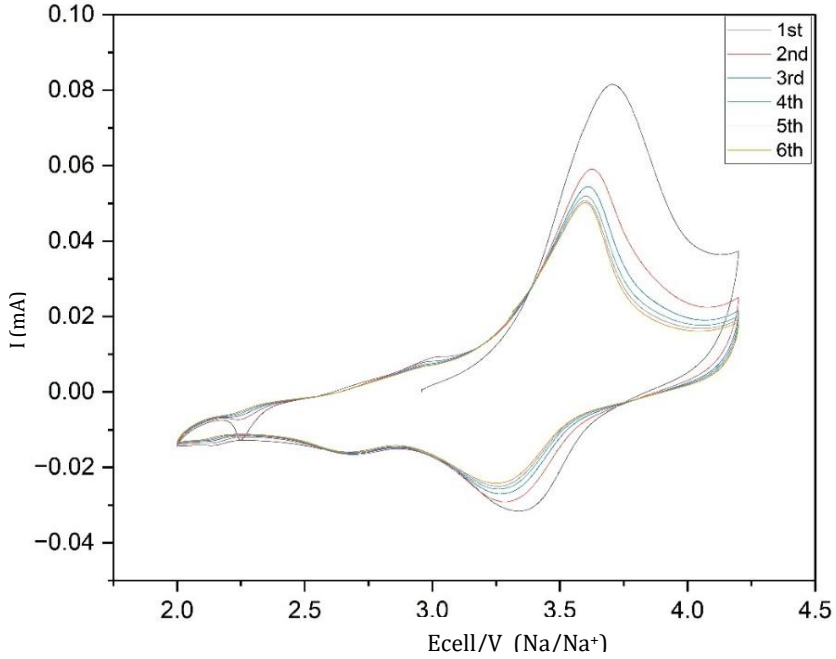

Figure 14 - Cyclic-voltammetry (CV) profile displaying distinct redox peaks near 3.1 and 3.4 V

4.4 Comparative Discussion

4.4.1 Structural Comparison (XRD Analysis)

A comprehensive comparison of the three synthesis techniques co-precipitation, self-decomposition, and hydrothermal clearly demonstrates the crucial influence of synthesis conditions on the structural, morphological, and electrochemical behaviour of the Fe–Mn–Co–Cu–Ni multi-metal PBA's (PBAs). The X-ray diffraction (XRD) patterns of all three samples confirmed the formation of the face-centred cubic (Fm-3m) structure typical of PBAs, without the appearance of any impurity peaks, verifying successful incorporation of all five transition-metal species into a single framework. However, significant differences in crystallinity and lattice order were observed depending on the synthesis route. The self-decomposed sample exhibited the sharpest and most intense diffraction peaks, signifying superior crystallinity, a highly ordered framework, and minimal lattice strain. This behaviour can be attributed to the slow and controlled ion release during the decomposition of the precursor, which allows uniform metal incorporation and gradual crystal growth. The hydrothermal sample also displayed distinct diffraction peaks with reasonably high intensity, indicating good crystallinity, though minor peak broadening and slight intensity reduction suggested the presence of residual strain due to temperature-induced lattice stress or heterogeneous cation distribution under high-pressure synthesis conditions. In contrast, the co-precipitated sample produced broader and less intense peaks, reflecting small crystallite size and partial lattice disorder arising from instantaneous nucleation during rapid mixing of multiple transition-metal ions. These structural variations directly correlate with the growth kinetics of each method, confirming that slower, diffusion-controlled synthesis promotes long-range order and lattice stability, whereas fast precipitation yields defect-rich frameworks with limited atomic arrangement.

4.4.2 Morphological Comparison (SEM Analysis)

The differences in structure were further supported by morphological observations obtained from scanning electron microscopy (SEM). The co-precipitated product exhibited large, irregularly shaped particles with rough, fractured surfaces and extensive agglomeration, typical of a material formed through rapid and uncontrolled precipitation. The surface appeared porous and non-uniform, which can hinder effective electron pathways and restrict Na^+ diffusion through the electrode bulk. The self-decomposed sample presented a highly uniform cubic morphology with smooth surfaces and sharp edges, with individual particles ranging from 200 to 500 nm. The homogeneity of shape and size indicated controlled nucleation and isotropic growth, resulting in compact, well-connected grains that promote efficient ionic and electronic conductivity. The hydrothermal sample showed a distinctly different morphology, comprising spherical-to-polyhedral nanoparticles (100–300 nm) distributed uniformly but with slight aggregation. The smaller particle size and larger surface area provide greater electrode–electrolyte contact and potentially enhance charge-transfer kinetics; however, partial agglomeration and residual moisture can increase interfacial resistance and reduce long-term structural stability. Thus, while the hydrothermal route improved particle size control compared with co-precipitation, it did not achieve the degree of morphological uniformity and defect minimization realized in the self-decomposition process.

4.4.3 Electrochemical Comparison (CV and GCD Analysis)

The electrochemical response of the three materials, evaluated through cyclic-voltammetry (CV) and galvanostatic charge–discharge (GCD) testing, confirmed the impact of structural and morphological differences on sodium-ion storage performance. All samples exhibited two distinct redox peaks at approximately 3.1 V and 3.4 V, corresponding to the Fe^{2+}/Fe^{3+} and mixed Mn^{2+}/Mn^{3+}–Co^{2+}/Co^{3+} couples, characteristic of the redox activity of multi-metal PBAs. The self-decomposed electrode displayed sharp, symmetric, and highly stable peaks with minimal voltage separation, indicating fast redox kinetics, low polarisation, and excellent reversibility. The hydrothermal electrode also exhibited well-defined peaks, though slightly broader and with a modest increase in separation, signifying moderate polarisation and slower charge-transfer kinetics. The co-precipitated electrode showed the broadest and least distinct peaks, accompanied by the largest voltage gap, consistent with sluggish ion diffusion through a structurally disordered lattice. The GCD curves mirrored these results: the self-decomposition sample produced flat, well-defined voltage plateaus between 3.2 V and 3.4 V, with the highest specific capacity of about 100 mAh g^{-1} and the best reversibility; the hydrothermal sample delivered an intermediate capacity of approximately 85 mAh g^{-1} with stable cycling; and the co-precipitated sample exhibited the lowest capacity of around 80 mAh g^{-1}, coupled with higher polarization and weaker voltage retention. Collectively, these findings reveal that the self-decomposition route, through its slower reaction kinetics and controlled crystal growth, produced the most ordered, compositionally homogeneous, and electrochemically active material. The hydrothermal method yielded a promising nanostructured morphology with acceptable crystallinity and scalability, whereas the co-precipitation route, despite being the simplest and most cost-effective, led to greater structural defects and lower Na^+-ion transport efficiency. Therefore, the overall performance hierarchy follows the order Self-decomposition > Hydrothermal > Co-precipitation, emphasising that precise control of synthesis kinetics and particle morphology is vital for optimising the structure–property relationship and achieving high-performance multi-metal PBA cathodes for sodium-ion battery applications.

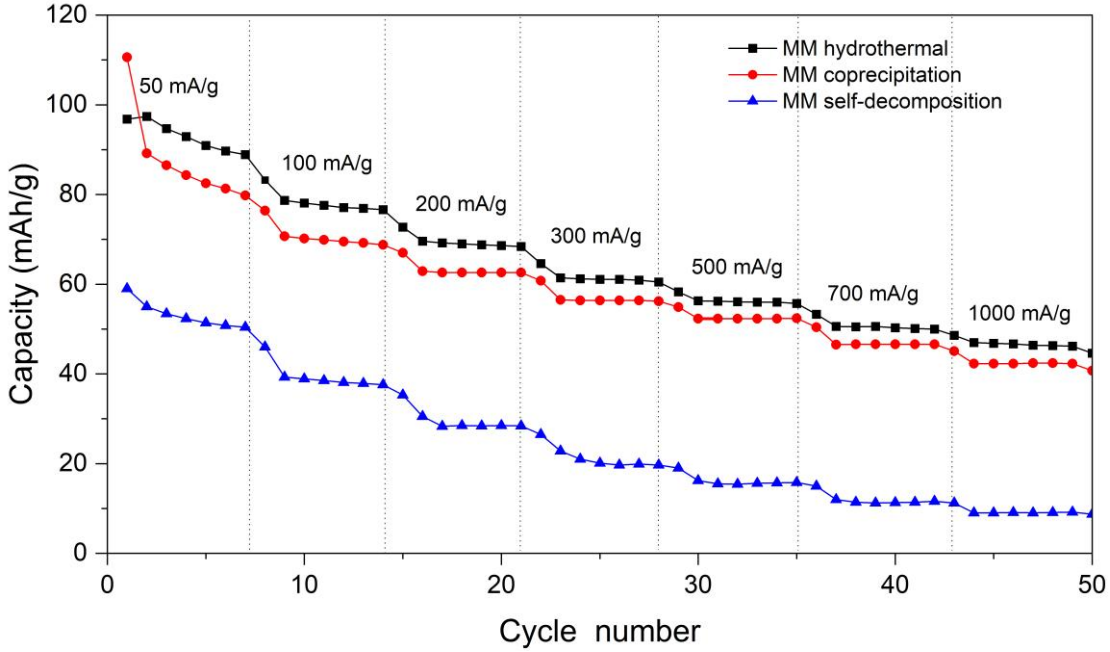

Figure 15 - Comparison of PBA samples from different methods

5 CONCLUSIONS AND FUTURE SCOPE

5.1 Conclusions

The comparative investigation successfully demonstrated that synthesis parameters play a pivotal role in governing the structure, morphology, and sodium-ion storage behaviour of multi-metal PBAs. All three synthesis routes produced single-phase, cubic Prussian Blue structures (Fm-3m), confirming that the incorporation of multiple transition metals (Fe, Mn, Co, Cu, Ni) into a single framework is both feasible and stable. However, their structural perfection and electrochemical performance varied markedly based on the synthesis environment and reaction kinetics. The self-decomposition method yielded the most promising results. Its slow and controlled ion-release mechanism during precursor decomposition facilitated homogeneous metal diffusion, resulting in highly crystalline, defect-free, and uniformly cubic particles (200–500 nm) with smooth surfaces and strong lattice connectivity. This structural uniformity minimised sodium-ion diffusion resistance and enhanced both ionic and electronic conductivity. Electrochemical testing showed that this sample achieved the highest specific capacity (~100 mAh g^{-1}), the most symmetric redox peaks, and the lowest polarisation, confirming superior reversibility and stability. The hydrothermal route, performed under elevated temperature and pressure, produced well-dispersed spherical-to-polyhedral nanoparticles (100–300 nm) with good crystallinity and stable electrochemical response. Its moderate specific capacity (~85 mAh g^{-1}) and consistent cycling stability make it a promising approach for scalable synthesis, though further optimisation is required to reduce residual strain and surface aggregation. The co-precipitation route, while the simplest and most cost-effective method, resulted in irregular particle morphology, lower crystallinity, and greater internal strain due to rapid precipitation and uncontrolled nucleation of multiple metal cations. These structural imperfections led to sluggish Na^+ diffusion and reduced redox efficiency, yielding the lowest specific capacity (~80 mAh g^{-1}) among the three methods.

Overall, the findings of this study clearly establish that the self-decomposition method is the most effective route for synthesising high-quality, compositionally homogeneous Fe–Mn–Co–Cu–Ni PBAs. The slow reaction kinetics inherent to this process enable precise structural control, improved lattice stability, and enhanced electrochemical reversibility, all of which are crucial for developing advanced sodium-ion battery cathodes. This work contributes valuable insights into the relationship between synthesis parameters, microstructural order, and sodium-ion transport dynamics in multi-metal PBA's.

5.2 Future Scope

While this research successfully established the influence of synthesis methods on the structure and performance of multi-metal PBAs, there remain several promising avenues for further investigation and optimisation:

1. **Long-term cycling and rate performance:**
   Future studies should extend charge–discharge testing over hundreds of cycles and at multiple current densities to evaluate the long-term stability and rate capability of the optimised self-decomposed material.

2. **Surface and elemental characterisation:**
   Advanced techniques such as X-ray photoelectron spectroscopy (XPS), energy-dispersive X-ray spectroscopy (EDS) mapping, and inductively coupled plasma (ICP) analysis can be used to confirm elemental distribution, oxidation states, and uniform metal incorporation across the PBA lattice.

3. **Optimisation of metal composition and stoichiometry:**
   Exploring variations in the Fe:Mn:Co:Cu: Ni ratio may further enhance redox potential, energy density, and cycling stability, offering scope for tailoring PBAs for specific voltage or power applications.

4. **Full-cell assembly and practical validation:**
   Integrating the optimised PBA cathode with a suitable anode (such as hard carbon or Na–Sn alloy) in a full sodium-ion cell would provide practical insights into real-world energy performance and scalability.

In conclusion, this research provides a comprehensive understanding of how synthesis mechanisms influence the physical and electrochemical behaviour of Fe–Mn–Co–Cu–Ni multi-metal PBAs. By establishing clear structure–property correlations and identifying the self-decomposition route as the most efficient synthesis strategy, this work lays a strong foundation for further development of sustainable, low-cost, and high-performance sodium-ion batteries for next-generation energy storage systems.

6 References

1. *Challenges and industrial perspectives on the development of sodium-ion batteries.* Cai, X., et.al. 2024, Journal of Alloys & Compounds.

2. *Low-cost Prussian Blue Analogues for sodium-ion batteries and other metal-ion batteries.* Huang, J., Du, R., Zhang, H., Liu, Y., Chen, J., Liu, Y., Li, L., Peng, J., Qiao, Y. & Chou, S. 2023, Chemical Communications, Vol. 59, pp. 9230-9335.

3. *Prussian Blue cathode materials for sodium-ion batteries and other ion batteries.* Qian, J., Wu, C., Cao, Y., Ma, Z., Huang, Y., Ai, X. & Yang, H. 2018, Advanced Energy Materials.

4. *Encapsulating Mn–Fe Prussian Blue Analogues nanocuboids into a graphene framework towards fast and durable sodium storage.* Dong, D., Han, B., Zhou, Y. & Deng, C. 2024, Materials Letters.

5. *Recent progress of manganese-based Prussian Blue Analogues cathode materials for sodium-ion batteries.* Liu, Y., Liu, Y., Zhang, H. & Zhang, Z. 2023, Ionics.

6. *Effect of crystal water on electrochemical performance and structural evolution of Prussian Blue Analogues cathodes.* Park, J., Lee, S. W., Kim, J. & Cho, B. W. 2023, Journal of Power Sources, Vol. 233192, p. 574.

7. *Prussian Blue Analogues for high-performance sodium-ion battery cathodes: recent advances and challenges.* Sun, S., Jiang, X., Wang, Z., Lei, H., Zhai, Y. & Wang, P. 2025, Dalton Transactions, Vol. 54, p. 14254.

8. *Effect of sodium content on electrochemical performance of Prussian Blue Analogues electrode materials for sodium-ion batteries.* Chen, W.-C., Xu, S.-H., Fei, G. T. & Ouyang, H. 2024, Solid State Ionics.

9. *Understanding capacity fading from structural degradation in Prussian Blue Analogues for wide-temperature sodium-ion cylindrical battery.* Zhang, H., Li, J., Liu, J., Gao, Y., Fan, Y., Liu, H., Chen, X., Wu, X. & Liu, Y. 2025, Nature Communications, Vol. 2520, p. 16.

10. *Prussian Blue Analogues for Sodium-Ion Battery Cathodes: Mechanistic Insights, Current Challenges and Future Pathways.* Xiao, Y., Xiao, J., Zhao, H. & Liu, H. 2024, Small, Vol. 2401957, p. 20.

11. *Prussian Blue Analogues for Aqueous Sodium-Ion Batteries: Research progress and challenges.* Wang, Y., et al. 2024, Advanced Energy Materials.

12. *Dominant role of M element on the stability and properties of $Na_xMFe(CN)_6$ (M = 3d transition metal) as cathode material for sodium-ion batteries.* Han, J., Lin, Y., Yang, Y. & Liu, X. 157430, 2021, Journal of Alloys and Compounds, p. 855.

13. *A low-defect and Na-enriched Prussian Blue lattice with ultralong cycle life for sodium-ion battery cathode.* Changxiu, Y., Zhao, A., Zhong, F. & Cao, Y. 2019, Electrochimica Acta, Vol. 301, pp. pp. 27-34.

14. *Understanding redox mechanisms in multi-metallic Prussian Blue Analogues for sodium-ion storage.* Chen, L., Zhang, W., Xu, H. & Guo, X. 2022, Electrochimica Acta, p. 425.

15. *Ball-milling synthesis of low-water and phase-stable Prussian Blue for sodium-ion batteries.* Cheng, H., Liu, Y.-N., Wang, D. & Guo, B. 2024, Solid State Ionics.

16. *The design and synthesis of Prussian Blue Analogs as a sustainable cathode for sodium-ion batteries.* Fan, S., Liu, Y., Gao, Y. & Chou, S.-L. 2023, Journal of Materials Chemistry A.

17. *Hydrothermal synthesis of defect-suppressed Fe–Mn–Co–Cu–Ni Prussian Blue Analogues for sodium-ion batteries.* Gao, L., Chen, X., Wang, F., Liu, Q. & Luo, J. 2024, Journal of Energy Chemistry, Vol. 90, pp. 220-231.

18. *Moisture-controlled Prussian White/CNT composite high-energy cathode for next-generation sodium-ion batteries.* Jeong, W., Baek, J., Kim, J.-K. & Lee, J. 2023, Materials Research Bulletin.

19. *Prussian Blue Analogues in sodium-ion batteries.* Komenda, A., et al. 2025, Renewable & Sustainable Energy Reviews.

20. *Prussian Blue/reduced graphene oxide composites cathode material via one-pot precipitation synthesis for enhancing capacity of sodium-ion pouch cell batteries.* Kongthong, T., Poochai, C., Tuantranont, A. & Sriprachuabwong, C. 2024, Journal of Industrial and Engineering Chemistry.

21. *Synergistic electronic and ionic enhancement of nickel hexacyanoferrate for robust sodium-ion battery performance under extreme condition.* Li, J., Zhang, Z., Yuan, Q. & Wang, C. 2025, Journal of Power Sources.

22. *Synthesis of low-defect iron-based Prussian Blue with enhanced performance for sodium-ion batteries.* Li, Z., et al. 2025, Materials, p. 1455.

23. *Gradient doping–induced triphasic intergrowth hexacyanoferrate cathode for high-performance sodium-ion batterie.* Lin, X., Chen, G., Xu, X. & Wu, X. 2024, Chemical Engineering Journal.

24. *Modified multi-metal Prussian Blue Analogues toward high-performance cathode for sodium-ion battery.* Nguyen, T.X., et al. 2024, Journal of Alloys and Compounds.

25. *Experimental and computational optimization of Prussian Blue Analogues as high-performance cathodes for sodium-ion batteries: A review.* Oh, G., Kim, J., Kansara, S. & Hwang, J.-Y. 2024, Advanced Energy Materials.

26. *High-entropy activated and stabilized nickel-based Prussian Blue Analogues for high-performance aqueous sodium-ion batteries.* Ran, B., Cheng, R., Zhong, Y. & Fu, C. 2024, Colloids and Surfaces A: Physicochemical and Engineering Aspects.

27. *Degradation Mechanisms of Prussian Blue Analogues and their implications for sodium-ion batteries.* Sterzinger, J., et al. 2025, Journal of Physical Chemistry C.

28. *Prussian Blue Analogs for Rechargeable Batteries: Progress and Challenges.* Wang, B., et al. 2018, Materials Research Bulletin.

29. *High-entropy Prussian Blue Analogues with 3D confinement effect for long-life sodium-ion batteries.* Wu, J., Wang, G., Li, K. & Guo, C. 2024, Journal of Colloid and Interface Science.

30. *$Na_2Ni_xCo_{1-x}Fe(CN)_6$: a class of Prussian Blue Analogues with transition-metal elements as cathode materials for sodium-ion batteries.* Xie, M., Huang, Y., Xu, M., Chen, R., Zhang, X., Li, L. & Wu, F. 2016, Electrochemistry Communications, Vol. 59, pp. 91-94.

31. *Electrochemistry of polynuclear transition metal cyanides: Prussian Blue and its Analogues.* Itaya, K., Uchida, I. & Neff, V. D. s.l. : Accounts of Chemical Research, 1936, Vols. 162–168.

32. *Prussian blue Analogues as cathode materials for sodium-ion batteries.* You, Y. et al. s.l. : Advanced Energy Materials, 2018, Vol. 1701785.

33. *Defect engineering of Prussian Blue cathodes for sodium-ion batteries.* Wang, L. et a. s.l. : Energy Storage Material, 2019, Vols. 37–45.

34. *Hydrothermal synthesis of low-defect Prussian Blue cathodes.* Zhang, W. et al. s.l. : Journal of Materials Chemistry A, 2020, Vols. 16019–16027.

35. *Multi-metal Prussian Blue Analogues for enhanced sodium storage.* Zhou, A. et al. s.l. : ACS Applied Materials & Interfaces, Vols. 12032–12041.

36. *Entropy-stabilized multi-metal Prussian Blue Analogues.* Li, H. et al. s.l. : Advanced Functional Materials, 2022, Vols. 32, 2109813.

37. *Towards high energy density sodium-ion batteries.* Ponrouch, A. et al. s.l. : Energy & Environmental Science, 9, 2016, Vols. 2381–2389.

38. *Sodium-ion batteries.* Slater, M. D. et al. s.l. : Advanced Functional Materials, 2013, Vols. 23, pp. 947–958.

39. *The mechanisms of sodium and lithium insertion in carbon materials.* Stevens, D. A. & Dahn, J. R. s.l. : Journal of The Electrochemical Society, 2001, Vols. A803–A811.

40. *Recent development on Na-ion batteries.* Bommier, C. & Ji, X. s.l. : Small, 2013, Vols. 14, 1703576.

DEPARTMENT OF XXXX XXXXXXXXXXX
XXXXXXXX XXXXXXXXXXX XX
CHALMERS UNIVERSITY OF TECHNOLOGY
Gothenburg, Sweden 20xx
www.chalmers.se

CHALMERS
UNIVERSITY OF TECHNOLOGY